Supplementary Materials for

Reengineering chimeric antigen receptor T cells for targeted therapy of autoimmune disease

Christoph T. Ellebrecht, Vijay G. Bhoj, Arben Nace, Eun Jung Choi, Xuming Mao, Michael Jeffrey Cho, Giovanni Di Zenzo, Antonio Lanzavecchia, John T. Seykora, George Cotsarelis, Michael C. Milone,* Aimee S. Payne*

*Corresponding author. Email: aimee.payne@uphs.upenn.edu (A.S.P.); milone@mail.med.upenn.edu (M.C.M.)

Published 30 June 2016 on *Science* First Release
DOI: 10.1126/science.aaf6756

This PDF file includes:

Other Supplementary Material for this manuscript includes the following:
(available at www.sciencemag.org/cgi/content/full/science.aaf6756/DC1)

Materials and Methods

Cell lines and antibodies

AK18, AK19, and AK23 PV hybridomas were a gift from Prof. Masayuki Amagai, Keio University. BK2 control hybridoma targeting human VH3-15 (*38*) (HB11720), Nalm-6 and 293T (CRL-11268) cells were obtained from ATCC. HaCat keratinocytes were provided by Prof. John T. Seykora (University of Pennsylvania). The Jurkat T cell line was provided by Arthur Weiss (University of California, San Francisco). Primary human T cells, peripheral blood mononuclear cells, and bone marrow aspirates from healthy donors were provided by the Human Immunology Core at the University of Pennsylvania. Primary human keratinocytes were obtained from neonatal foreskins according to Institutional Review Board approved protocols.

To engineer K562 cells (ATCC: CCL-243) (previously transduced to express CD19) or Nalm-6 cells to express surface IgG BCRs, CD79a and CD79b co-receptors were expressed by means of lentiviral transduction and sorted based on CD79b expression (Influx, BD) (Fig. S2C). CD79a/b positive cells were transduced with lentiviral vectors for surface expression of IgG of the human anti-Dsg3 clones F779 and PVB28 and sorted based on IgG expression. Dsg3-reactivity of the BCRs was confirmed by flow cytometry (Fig. S2D-F).

Human anti-Dsg3 antibodies Px43, Px44, F779, PVB28 were previously described (*39-41*). Px43 and Px44 IgG1 were produced as described (*42*, *43*). Px44 was additionally produced as scFv as previously described (*39*) and labeled with AF647 (Thermo Fisher) according to the manufacturer's recommendations. Px44 binds Dsg3 in the presence of EDTA and can therefore be used in K2-EDTA anticoagulated blood samples to detect Dsg3 CAAR-Ts. F779 and PVB28 IgG4 were synthesized (IDT) as single transcripts with furin and F2A sites separating 6xHis-tagged heavy chains and V5-tagged light chains, then cloned into pcDNA6 (Life Technologies) for transient transfection into 293T cells. F779 and PVB28 IgG4 were purified using Talon (Clontech) beads after buffer exchange into 300mM NaCl, 50mM sodium phosphate buffer pH 7.0. AK18, AK19, and AK23 hybridomas were cultured in PFHM-II (Life Technologies) containing 0.25% cholesterol, and antibodies were purified from the culture supernatant using protein G agarose. CAARs were detected by flow cytometry using the aforementioned antibodies which were detected with either anti-human IgG-Fc (clones: HP6017, G18-45)-PE or anti-mouse IgG1 (clone: A85-1)-PE or APC. In some instances the kappa or lambda light chains of the human antibodies were used for detection (clone: MHK-49, APC, Biolegend; lambda as negative control for F779, PVB28 IgG: clone: MHL-38, PE, Biolegend). Sera from PV patients were collected according to Institutional Review Board approved protocols. Antibodies for flow cytometry are described below. Mycoplasma contamination was ruled out twice annually. After cell sorting, cells were cultured in medium prophylactically supplemented with Plasmocin (Invivogen) for 2-3 passages. Additionally, hybridoma cell lines (AK18, AK19, AK23) were empirically treated with Plasmocin (Invivogen) for 4 weeks before experimentation.

Design and construction of the Dsg3 CAAR

We cloned the full length Dsg3 CAAR by PCR amplification of DNA fragments from human peripheral blood mononuclear cell genomic DNA or cDNA or codon-optimized synthesized DNA (GeneArt, Life Technologies) with primers as outlined in Table S1. Fragments were gel purified and subjected to extension overlap PCR to assemble the complete Dsg3 CAAR

fragment. We cloned the Dsg3 CAAR into a third generation lentiviral vector, pRRLSIN.cPPT.PGK-GFP.WPRE (Addgene #12252), in which we had first replaced the PGK promoter with the human EF1α promoter. The initial Dsg3 EC1-5 CAAR included the endogenous Dsg3 propeptide and CD8 hinge, but subsequent constructs used the CD8 signal peptide and replaced the CD8 hinge with a 13 amino acid glycine-serine linker, with a unique NheI site that would allow subsequent cloning of extracellular domains using the BamHI-NheI sites.

For control CARs, single chain variable fragment (scFv)-based CARs against human CD19 (clone: FMC63) (*44*), HIV-1 gp120 (clone: VRC01) (*45*), and mesothelin (clone: SS1) (*46*) were synthesized and cloned into lentiviral vectors to express functional CARs in primary human T cells (Fig. S4). FMC63 and SS-1 were fused to a CD8 hinge and CD137 and CD3ζ cytoplasmic domains, VRC01 was followed by an IgG4-Fc (CH2+3), CD137 and CD3ζ cytoplasmic domains. Px44 was incorporated into a DAP-12-based, multichain immunoreceptor (DAP12-KIRS2) (*47*).

Target cell BCR expression quantification

To quantitate the density of surface BCRs on target cells in comparison to primary human memory B cells, we stained K562-IgG$^+$ or Nalm-6 B cells and primary human B cells with anti-human IgG (clone G18-45, BD)-PE (fluorescence to protein (F/P) ratio ~1) under saturating conditions for 25 minutes at room temperature. After 2 washes in PBS, the cells were analyzed by flow cytometry (LSRII, BD) and the mean fluorescence intensity was calculated with FlowJo (Treestar). PV hybridoma cells were analyzed similarly using anti-mouse IgG (clone A85-1, BD)-PE (F/P ratio~1). To quantify the number of PE molecules per cell, PE quantibrite beads (BD) were analyzed on the same day with the same settings according to the manufacturer's recommendations. To calculate the BCR density per cell, the cell surface of PV hybridomas, K562, Nalm-6 cells and primary human B cells was assessed with a Coulter Counter (Beckman Coulter). Density was calculated as PE molecules per μm^2.

Lentiviral production

VSV-G pseudotyped lentiviral particles were produced using a 4th generation packaging system. 293T cells (as these are commonly used for lentivirus production) were transfected at a confluency of 90% with a mixture of the pRRLSIN.cPPT.EF1α-gene-of -interest.WPRE, the envelope plasmid pMD2.G (Addgene #12252), the packaging plasmids pRSVRev (Addgene #12253) and pMDLgm/pRRE (Addgene #12251) in a complex with Lipofectamine 2000 (Life Technologies). Lentivirus containing supernatant was harvested after 24 and 48 hours, filtered through a 0.4 micron PES membrane, concentrated at 12,000xg for 12 hours at 4°C and stored at -80°C.

Stimulation and expansion of primary human T cells

Primary human T cells were cultured in RPMI1640, 10% FBS, 10 mM HEPES, 1% penicillin/streptomycin. Bulk T cells (CD4$^+$ and CD8$^+$) were stimulated with anti-CD3 and anti-CD28 beads (Dynabeads, Life Technologies) at a bead:cell ratio of 3:1. The culture medium was supplemented with 100 IU/mL interleukin 2. 24 hours after stimulation, 10^6 T cells were transduced with CAAR or control constructs or mock transduced. Expansion of the T cells was

monitored for 8-12 days by measurement of cell volume and concentration (Coulter counter, Beckman Coulter) (Fig. S1F,G). Cell surface expression of the CAAR constructs was validated by flow cytometry (BD LSRII) with aforementioned antibodies against Dsg3 (Fig. S1B,C). CAAR expression was quantified by staining with PVB28 IgG4 (100μg/ml) for 25 minutes at room temperature. Subsequently, after washing twice, bound human antibodies were detected with anti-human IgG (clone: G18-45) and the antibody-binding capacity was quantified with Quantum Simply Cellular beads (Bangs Laboratories). All staining procedures were performed under saturating conditions. CAAR-T cells and quantification beads were analyzed by flow cytometry and the antibody binding capacity was calculated with QUICKCAL (Bang Laboratories) (Fig. S1E). For some experiments, transduced T cells were previously frozen in 90% FBS and 10% DMSO. Experiments were performed when cells were rested after stimulation (i.e. volume of <450fl).

Proliferation was quantified with the carboxyfluorescein diacetate succinimidyl ester (CFSE) dilution method. CAAR-T cells were labeled in PBS-1 mM Ca^{2+} at a density of 10^7 /ml with CFSE (1 μM) for 5 minutes at room temperature. The reaction was quenched by adding PBS-10% FBS. After washing twice in PBS-Ca^{2+}-10%FBS, T cells were adjusted to a concentration of $1x10^6$/ml and stimulated in a volume of 400μl with either anti-CD3/anti-CD28 beads (Dynabeads, ThermoFisher), soluble anti-Dsg3 monoclonal antibodies at a concentration of 100μg/ml, normal human IgG (Privigen) (10 mg/ml), or PV serum from a patient off therapy (Dsg3 ELISA index 180 U/ml). Unlabeled and labeled cells that were left unstimulated were used as controls. Proliferation was assessed after 96 hours by flow cytometry after staining dead cells with 7-AAD (BD). Cultures were set up in duplicate. After 48 hours, 100 μl of the culture supernatant was removed to assess cytokine production by ELISA.

Analysis of CAAR-mediated signaling with NFAT-GFP Jurkat reporter T cells

To test signal transduction by CAAR-target interaction, the CAAR constructs were expressed in a Jurkat reporter cell line selected with G418 for stable expression of GFP controlled under an NFAT response element, which results in GFP expression after CAAR engagement and phospholipase Cγ/IP3-mediated intracellular calcium release (*48*). Jurkat cells were transduced with CAAR lentivirus at a multiplicity of infection of 5-10 and expression of the CAAR construct was validated after >72 hours by flow cytometry. As a positive control for Dsg3 expression and chimeric immunoreceptor engagement, Jurkat cells were transduced with an anti-Dsg3/1 antibody-based Px44 CAR (Fig. S4), which binds Dsg3 and Dsg1 expressed on primary human keratinocytes. For characterization of CAAR-target interaction, the CAAR Jurkat cells were incubated for 4-16 hours with target cells at a ratio of 3:1 or with soluble anti-Dsg3 monoclonal antibodies or okt3 (Biolegend) at a concentration of 50μg/ml. GFP expression was validated by flow cytometry (LSRII, BD). In addition to the target cells, primary human keratinocytes were used to test for off-target effects. Primary human keratinocytes were co-incubated with $2\text{-}5x10^5$ Jurkat reporter cells at confluencies from 50-100% and after increasing the Ca^{2+} concentration to 1 mM for 16-72 hours to induce Dsg3 surface expression.

Flow-cytometry based sorting of bone marrow B cells

Flow-cytometry based cell sorting of bone marrow aspirate cells from healthy donors was performed by isolating mononuclear cells by Ficoll-Paque (GE Healthcare Bio-sciences, Pittsburgh, PA) density centrifugation. Cells were then surface stained using the following antibodies: anti-CD3 APC-Cy7 (clone: SP34-2), anti-CD14 APC-H7 (clone: M5E2), anti-CD16 APC-H7 (clone: 3G8), anti-CD20 PerCP (clone: L27), anti-CD38 BV605 (clone: HB7), anti-CD45 FITC (clone: HI30), anti-CD138 BV421 (clone: MI15) all from BD Biosciences (Franklin Lakes, NJ), and anti- CD19 PE-Cy7 (clone: J3-119, Beckman Coulter, Pasadena, CA). Cells were then stained for viability using eFluor780 (eBioscience, San Diego, CA). Sorting was performed using a FACSAria (BD Biosciences, Franklin Lakes, NJ). Bone marrow B cells with the exception of plasma cells were defined and sorted as live, $CD3^-$, $CD14^-$, $CD16^-$, $CD38^-$, $CD138^-$ $CD20^+$ events. B cells and events obtained in the 'dump' channel ($CD3^+$, $CD14^+$, $CD16^+$) were coincubated with either Dsg3 CAAR, CD19 or non-transduced NFAT-GFP reporter Jurkat T cells for 16 hours at an E:T ratio of 3:1. GFP expression was analyzed by flow cytometry (LSRII, BD) and quantified with FlowJo (Treestar).

Surface stain of Dsg3-specific target cells

The extracellular portion of human Dsg3-Avitag was co-expressed with BirA under a polyhedrin promoter in a bicistronic vector (*49*). Human Dsg3-Avitag was produced by transfection and amplification in Sf9 cells and production in High Five cells using 50 μM D-biotin supplementation in the culture medium. For staining anti-Dsg3 BCR expressing target cells, $5x10^5$ cells were resuspended in 200ul sterile-filtered High Five cell supernatant and incubated at room temperature for 25 minutes. After washing twice, biotinylated Dsg3 was detected with Streptavidin-PE (0.25 μg/ml, BD) after 25 minute incubation at room temperature and 2 additional washes. Staining specificity was optimized by titration of Streptavidin-PE concentration (Fig. S2D,E).

In vitro cytotoxicity and cytokine assays

In vitro killing of hybridomas, K562, Nalm-6 and HaCat cells was tested with a ^{51}Cr-release assay. $5x10^5$ target cells were loaded with 50 μCi of $Na_2{}^{51}CrO_4$ (Perkin Elmer) for 90-120 minutes, washed twice and resuspended in phenol red-free medium with 5% FBS. Dsg3 CAAR, control CAR, or mock transduced T cells (8-10 days after initial activation) were co-incubated with loaded target cells for 4 hours at various effector:target (E:T) ratios, and chromium release into the supernatant was measured with a MicroBeta2 plate counter (Perkin Elmer). Soluble antibodies were added to target cells at indicated concentrations to test inhibition of CAAR-T cells. To test killing in the presence of soluble, polyclonal serum IgG, PV IgG was purified from plasma with Melon gel (Thermo Fisher) according to the manufacturer's recommendations and buffer-exchanged into PBS (Amicon, Merck Millipore). Appropriate dilutions within the linear range of the Dsg3 ELISA with indices between 160 and 70 IU/ml were determined with a commercially available Dsg3 ELISA kit (Euroimmun). Killing assays in the presence of soluble monoclonal or polyclonal IgG were performed at an E:T of 30:1 with concentrations between 10-100 μg/mL, the physiologic range observed in most PV patients (*50*). Spontaneous release by target cells (without effector cells) was analyzed in the same volume, and maximum release was assessed by lysing target cells with SDS at a final concentration of

5%. Percent specific lysis = [(Experimental Release – Spontaneous Release)/ (Maximum Release – Spontaneous Release)] *100. All experiments were performed with at least 3 replicates, and with primary human T cells from >10 distinct donors.

To test redirected, Fc-receptor mediated lysis, K562 cells positive for CD64 (FcγRI) were incubated in serum from a PV patient (Dsg3 ELISA index >200 U/ml) for 30 minutes at room temperature, washed twice and loaded with chromium as mentioned above. After 2 additional washes $CD64^+$ K562 cells were resuspended in PV serum and added to effector T cells already cultured in PV serum.

Interferonγ production was quantified by ELISA (R&D) according to the manufacturer's recommendations in duplicate culture supernatants after co-culture of $3x10^5$ effector cells and 10^5 target cells in 400 µl for 24-96 h.

Planar lipid bilayers and total internal reflection (TIRF) microscopy

Glass supported planar lipid bilayers were prepared in FCS-2 flow cells (Bioptechs). Small unilamellar vesicles (SUVs) were created from DOPC and 25% DGS-NTA (Avanti). Organic solvents were removed in vacuum overnight and lipids were rehydrated in PBS by sonication. Rehydrated lipids were extruded through a 50nm pore membrane (Avanti) and stored at 4C. Piranha etched (H_2SO_4: H_20_2 2:1) glass slides were loaded with 1-2 µl SUVs (final NTA concentration: 12.5%) to induce bilayer formation. After charging with 100 µM $NiCl_2$ and blocking of the bilayer with 3% fetal bovine serum for 30 minutes , human ICAM-1 (1µg/ml) and anti-Dgs3 IgG4-12-His (PVB28 or F779, density: 250 molecules/μm^2) labeled with Alexa Fluor 647 (Life Technologies) were reacted with lipid bilayers. All buffers used in these experiments contained 1mM Ca^{2+} to keep the Dsg3 CAARs in their native conformation. FCS-2 flow cells were prewarmed to 37°C and EC1-4 CAAR Jurkat T cells were injected in PBS/Ca2+ supplemented with 3% fetal bovine serum. Jurkat cells were transduced with either CD45-GFP or actin-GFP and sorted by flow cytometry. EC1-4 CAAR tagged with mCherry was lentivirally transduced into CD45-GFP or actin-GFP Jurkat cells. Cells were cultured as described above and injected into the flow cell in PBS/Ca^{2+} at a density of $5x10^6$ cells/ml. After injection, cells were imaged immediately and for up to 90 minutes at 37°C (µ environment controller, Bioptechs). TIRF imaging was performed using an Apo TIRF 100x Oil 1.49 NA objective, Andor iXon EMCCD camera, 491 nm, 561 nm and 633 nm lasers, FITC/Cy3/Cy5 emission filters, SRIC cube (IRM), a programmable mechanized stage, and infrared autofocus (Perfect Focus) on a Nikon Eclipse Ti inverted fluorescence microscope automated with NIS-Elements software. The contact plane between cell and bilayer was confirmed by focusing in SRIC mode (Nikon). For real-time experiments, images were acquired every 3 seconds for 60-70 minutes. ImageJ-FIJI (NIH) was used for analysis of images. At indicated time points, cells were fixed by injection of 4% paraformaldehyde into the flow cell. Protein densities were quantified by coating 5µm silica beads (Bangs Laboratories Inc.) with lipid bilayers and indicated proteins at various concentrations. Densities were calculated in comparison to Quantum AF647 MESF calibration beads (Bangs Laboratories Inc.) according to the manufacturer's recommendations after acquisition by flow cytometry (BD, LSRII).

Surface antibody binding competition assay

To detect antibody retention, CAAR-T cells (EC1-4) were incubated with biotinylated AK18, AK19, AK23, F779 IgG4 or PVB28 IgG4 (20μg/ml) for 20 minutes on ice. Cells were washed twice and incubated at 37°C or 4°C in medium with fivefold excess of soluble, non-biotinylated antibody (i.e. 100μg/ml). At indicated time points, cells were washed and stained with streptavidin-PE for 20 minutes at room temperature before assessment of retained biotinylated antibody was quantified by flow cytometry (BD LSRII). Mean fluorescence intensity was calculated with FlowJo (Treestar), and the proportion of IgG-retaining cells was determined in relation to cells at the time point 0.

Surface plasmon resonance

All experiments were performed with a BiacoreX (Biacore, Inc) optical biosensor at 25°C in TBS 1 mM $CaCl_2$ running buffer as previously described (*40*) with the following modifications. Anti-human IgG and anti-mouse IgG were immobilized on a CM5 chip according to manufacturer's instructions (GE Healthcare, Antibody Capture Kit). Mouse and human IgG were immobilized with the respective capture antibodies resulting in immobilization levels of ~150 RUs. For kinetic measurements of IgG binding to Dsg3, conformational, mature Dsg3 (Euroimmun) was injected at indicated concentrations (nM) using a flow rate of 50 μl/min, 2 minutes association time, and 3-5 minutes dissociation time. The sensor surface was regenerated with 10 mM glycine-HCl pH 2.5. Flow cells with anti-mouse and anti-human IgG alone were used as a reference for background binding subtraction. Off-rate, on-rate and binding constants were calculated after background subtraction with BIAevaluation 3.0 (Biacore) software using a 1:1 Langmuir binding model with separate fit for association and dissociation.

PV hybridoma and Nalm-6 *in vivo* CAAR-T xenograft experiments to evaluate CAAR-T efficacy

NOD-scid-gamma (NSG; NOD.Cg-*Prkdc*^{scid} *Il2rg*^{tm1Wjl}/SzJ) mice, which lack an adaptive immune system, were obtained from the Jackson Laboratory (Bar Harbor) or bred in house under an approved institutional animal care and use committee protocol and maintained under pathogen-free conditions. Animals were assigned in all experiments to treatment/control groups based on an urn randomization approach. All animals were included in endpoint analyses. Hybridoma cells were transduced with lentiviral vectors expressing click-beetle green or click-beetle red luciferase and GFP. 10 days after transduction GFP^+ IgG^+ cells were sorted by flow cytometry (BD Aria). Hybridomas were sorted on a regular basis to ensure persistence of the luciferase and surface IgG expression over several passages.

To test efficacy of CAAR-T cells against polyclonal PV hybridomas, AK18, AK19 and AK23 were mixed at equal proportions and a total number of $2x10^5$ hybridoma cells was injected intravenously into NSG mice (age 6-8 weeks), after pre-treatment of mice daily for 2 days with 600 mg/kg intravenous immunoglobulin (IVIG, Privigen) to minimize FcγR-mediated toxicity against hybridoma cells. After 5 days, a mixture of EC1-3 and EC1-4 Dsg3 CAAR T cells (10^7 cells per mouse) were injected intravenously in a final volume of 200 μl. Bioluminescence was quantified with an Xenogen IVIS spectrum (Caliper Life Sciences) on day 1, 4, 7, 9, 11, 14, and 18 after injection. To do so, D-Luciferin potassium salt (Thermo Fisher) was injected

intraperitoneally at a dose of 150mg/kg body weight, which was combined with intraperitoneally administered IVIG (600 mg/kg). Mice were anaesthetized with 2% isoflurane and luminescence was assessed 10 minutes after injection in automatic exposure mode. Total flux was quantified using Living Image 4.4 (PerkinElmer) by drawing rectangles of identical area around mice reaching from head to the 50% of the tail length; background bioluminescence was subtracted for each image individually.

Serum samples for antibody quantification were obtained by retro-orbital bleeding on day 5 and day 14 in serum-separator tubes (BD), processed according to the manufacturer's recommendations and stored at -80^{o}C. Serum antibody titers were determined by Dsg3 ELISA (Euroimmun) at a serum dilution of 1:10 (AK18, AK19 and AK23). Serum anti-Dsg3 antibodies were detected with donkey anti-mouse IgG (H+L)-HRP (Abcam). Complete blood counts were obtained with a Hemavet 1700 counter (Drew Scientific) from K2-EDTA blood samples at the end of each experiment.

To test efficacy of CAAR T cells against monoclonal PV hybridomas, AK18, AK19 and AK23, CAAR T cells were co-engrafted with hybridoma cells into NSG mice. For this purpose, 1-2x10^{5} hybridoma cells were mixed and kept on ice with 3-4x10^{6} CAAR T cells and injected intravenously in a final volume of 200µl. Bioluminescence was quantified with an Xenogen IVIS spectrum (Caliper life sciences) on day 0, 3, 7, 13, and 18 after injection. Serum samples for antibody quantification were obtained by retro-orbital bleeding on day 10 and at the end of each experiment in serum-separator tubes (BD), processed according to the manufacturer's recommendations and stored at -80^{o}C. Serum antibody titers were determined by ELISA against human Dsg3 (Euroimmun) at a serum dilution of 1:10 (AK18, AK23) and 1:20 (AK19). Serum anti-Dsg3 antibodies were detected with donkey anti-mouse IgG (H+L)-HRP (abcam).

After injection of hybridomas and CAAR-T cells, animals were clinically monitored for signs of graft-versus-host disease and other toxicity as evidenced by >10% weight loss, loss of fur, diarrhea, conjunctivitis, or leukemia-related hind-limb paralysis. In initial studies, intravenous injection of hybridoma doses between 5x10^{4} and 10^{6} cells result in a 200- to 2000-fold expansion and death (or severe toxicity requiring euthanasia) beginning at 3 weeks. A 1000-fold expansion was observed between day 7 and day 17 (Fig. S8A), indicating an *in vivo* doubling time of approximately 24 hours. Because death is an inhumane endpoint, a total flux of 10^{8} photons/second, indicating a >100-fold expansion of the target cells compared to the initial burden and therefore loss of disease control, was defined as the study endpoint. Control and Dsg3 CAAR-T treated mice were euthanized 18-25 days after hybridoma/T cell injection; in some experiments Dsg3 CAAR-T treated mice were allowed to progress longer to determine mechanisms of escape in Dsg3 CAAR-T treated mice.

To test CAAR efficacy in the Nalm-6 B cell model, Nalm-6 B cells were transduced with a lentiviral vector expressing CD79a and CD79b (as they are lacking their endogenous expression, which is required for cell surface BCR presentation (*51*)), sorted for CD79b (clone: CB3-1, Southern Biotech) expression (BD Aria), and re-transduced with a lentiviral vector encoding PVB28 or F779 IgG BCR (Fig. S2A,B). Finally, cells were transduced with click-beetle green luciferase and GFP expressing vectors and sorted for GFP expression.

Mice were pretreated with IVIG (Privigen, CSL Behring) at a dose of 600 mg/kg i.v. for 2 days in order to block FcγRs on monocytes and neutrophils, which has been shown to be sufficient to enable engraftment of IgG4-Fc expressing T cells (*52*) and was required to enable

Nalm-6 IgG^+ engraftment. On day 3, mice were injected via the tail vein with 10^6 Nalm-6 B cells expressing F779 and PVB28 IgG mixed in equal proportions in 0.2 ml sterile PBS. T cells were injected via the tail vein at 5×10^6 in a volume of 0.2 ml of sterile PBS/Ca^{2+} 5 days after injection of Nalm-6. Nalm-6 at this dose produces fatal leukemia in NSG mice within 25 days if left untreated (*53*). As with the PV hybridoma model, because death is an inhumane endpoint, total flux $>10^{10}$ photons/s was used as the study endpoint for Nalm-6 experiments based on initial studies comparing bioluminescence flux with the timeframe for when death begins to occur or euthanasia becomes necessary.

Peripheral blood was obtained by retro-orbital bleeding, and the presence of B cells and T-cell engraftment was determined by flow cytometry using BD TruCOUNT (BD Biosciences) tubes as described in the manufacturer's instructions. Bioluminescence was assessed on day 5, 6, 7, 10, 13 and 18 after B cell injection, which was combined with intraperitoneally administered IVIG (600 mg/kg). For both models, mice were euthanized for organ harvest according to local IACUC guidelines, and bone marrow, spleen and blood samples were assessed by flow cytometry. Heart, gut, kidney, lung, liver and skin tissue was fixed in 4% formalin and processed by the pathology core of the University of Pennsylvania.

Animal experiments were periodically performed/assessed by blinded investigators, including bioluminescence imaging experiments, serum anti-Dsg3 ELISA assays, and tissue harvests.

Flow cytometry based ex vivo analysis of T cells, hybridoma cells, and Nalm-6 cells

Flow-cytometry based analysis of T cells, PV hybridoma cells and Nalm-6 cells was performed from flushed bone marrow, homogenized spleen and blood obtained at the end of each experiment. Cells were surface stained using the following antibodies: anti-CD3 BV711 (clone: okt3), anti-CD19 BV650 (clone: HIB19), anti-CD4 BV515 (clone: okt4), anti-CD45 APC-Cy7 (clone: HI30), all from BioLegend, and anti-CD8 APC-Cy5.5 (clone: RFT8, Southern Biotech), anti-mouse IgG PE or APC (clone A85-1, BD). Whole blood was then stained in Trucount tubes (BD) and fixed with FacsLyse solution (BD) according to the manufacturer's recommendations. Spleen and bone marrow samples were stained in RPMI, 3%FBS. Unless Trucount tubes were used, cell numbers were quantified with countbright absolute counting beads (Thermo Fisher).

Human skin xenografts

Human neonatal foreskins were obtained from the newborn nursery according to IRB-approved protocols and grafted to mice within 36 hours of collection as previously described (*54*). Grafts were allowed to heal for 7-9 weeks, then 10^6 T cells (Dsg3EC1-4 CAAR, Px44, or CART19) were injected intravenously into xenografted NSG mice. 2 mm punch biopsies of the grafts were performed on day 3. T cell engraftment was confirmed by flow cytometry on day 5 and day 18 as mentioned above. Skin biopsies were fixed in 4% paraformaldehyde for 16 hours at 4C, grossed and transferred into 70% ethanol before further processing for paraffin embedding and H&E/immunohistochemistry staining. Epidermal and dermal T cell infiltration was quantified with the ITCN plug-in (Center for Bio-Image Informatics, UC Santa Barbara) for FIJI/ImageJ (NIH).

Statistical analysis

Unless otherwise indicated, the graphs represent the mean value +s.e.m.. If individual data points are represented, a horizontal line indicates the mean of the group. Statistical comparison between unrelated groups was performed with an unpaired 2-sided Mann-Whitney or Student's t-test. In the human skin xenograft experiment, epidermal T cell infiltration was compared to dermal infiltration with a paired ratio t-test. Survival or the time until the pre-determined threshold was reached in the hybridoma and Nalm-6 mouse model was compared with a log-rank (Mantel-Cox) test. Kaplan-Meier statistical analysis was used to determine whether treatment with the Dsg3 CAAR decreases disease burden by BLI. Our expected outcome was that 100% of untreated mice would die, whereas ≥75% of Dsg3 CAAR-treated mice would live. Even if 10% of untreated mice survived, the sample size had >85% power to detect a difference, calculated by log-rank test and assuming alpha error of 0.05. Unless otherwise indicated, asterisks in graphs represent as follows: *$p<0.05$, **$p<0.01$, ***$p<0.001$, ****$p<0.0001$. P values <0.05 were considered statistically significant. In flow cytometry plots, black crosses within a gate indicate the mean fluorescence intensity (MFI) of the gated population. Statistical analysis was performed with Prism (Graphpad software, v6.05).

Author contributions

CTE, VGB, MCM, ASP designed and performed experiments; AN, EJC, MJC, XM, GDZ, AL, JTS, GC assisted in experiments; CTE, VGB, MCM, ASP analyzed the data; CTE and ASP wrote the manuscript, MCM and ASP supervised the project and provided overall guidance; all authors reviewed and approved the final version of the manuscript.

References and notes

38. L. S. Berberian, Y. Valles-Ayoub, L. K. Gordon, S. R. Targan, J. Braun, Expression of a novel autoantibody defined by the VH3-15 gene in inflammatory bowel disease and Campylobacter jejuni enterocolitis, *J Immunol.* **153**, 3756 (1994).

39. A. S. Payne *et al.*, Genetic and functional characterization of human pemphigus vulgaris monoclonal autoantibodies isolated by phage display, *J. Clin. Invest.* **115**, 888 (2005).

40. M. J. Cho *et al.*, Shared VH1-46 gene usage by pemphigus vulgaris autoantibodies indicates common humoral immune responses among patients, *Nature Commun.* **5**, 4167 (2014).

41. G. Di Zenzo *et al.*, Pemphigus autoantibodies generated through somatic mutations target the desmoglein-3 cis-interface, *J Clin. Invest* **122**, 3781 (2012).

42. A. S. Payne, D. L. Siegel, J. R. Stanley, Targeting pemphigus autoantibodies by their heavy chain variable region genes, *J. Invest Dermatol.* **127**, 1681 (2007).

43. X. Mao *et al.*, MAPKAP kinase 2 (MK2)-dependent and -independent models of blister formation in pemphigus vulgaris, *J Invest Dermatol.* **134**, 68 (2014).

44. M. C. Milone *et al.*, Chimeric receptors containing CD137 signal transduction domains mediate enhanced survival of T cells and increased antileukemic efficacy in vivo, *Mol. Ther.* **17**, 1453 (2009).

45. X. Wu *et al.*, Rational design of envelope identifies broadly neutralizing human monoclonal antibodies to HIV-1, *Science.* **329**, 856 (2010).

46. R. Hassan *et al.*, Antitumor activity of SS(dsFv)PE38 and SS1(dsFv)PE38, recombinant antimesothelin immunotoxins against human gynecologic cancers grown in organotypic culture in vitro, *Clin Cancer Res.* **8**, 3520 (2002).

47. E. Wang *et al.*, Generation of Potent T-cell Immunotherapy for Cancer Using DAP12-Based, Multichain, Chimeric Immunoreceptors, *Cancer Immunol. Res.* **3**, 815 (2015).

48. E. Hooijberg, A. Q. Bakker, J. J. Ruizendaal, H. Spits, NFAT-controlled expression of GFP permits visualization and isolation of antigen-stimulated primary human T cells, *Blood.* **96**, 459 (2000).

49. S. Duffy, K. L. Tsao, D. S. Waugh, Site-specific, enzymatic biotinylation of recombinant proteins in Spodoptera frugiperda cells using biotin acceptor peptides, *Anal. Biochem.* **262**, 122 (1998).

50. T. Funakoshi *et al.*, Enrichment of total serum IgG4 in patients with pemphigus, *Br. J. Dermatol.* **167**, 1245 (2012).

51. T. E. Costa, R. R. Franke, M. Sanchez, Z. Misulovin, M. C. Nussenzweig, Functional reconstitution of an immunoglobulin antigen receptor in T cells, *J Exp. Med.* **175**, 1669 (1992).

52. M. Jonnalagadda *et al.*, Chimeric antigen receptors with mutated IgG4 Fc spacer avoid fc receptor binding and improve T cell persistence and antitumor efficacy, *Mol. Ther.* **23**, 757 (2015).

53. D. M. Barrett *et al.*, Treatment of advanced leukemia in mice with mRNA engineered T cells, *Hum. Gene Ther.* **22**, 1575 (2011).

54. L. A. Johnson *et al.*, Rational development and characterization of humanized anti-EGFR variant III chimeric antigen receptor T cells for glioblastoma, *Sci. Transl. Med.* **7**, 275ra22 (2015).

55. B. A. Schodin, T. J. Tsomides, D. M. Kranz, Correlation Between the Number of T Cell Receptors Required for T Cell Activation and TCR-Ligand Affinity, *Immunity* **5**, 137 (1996).

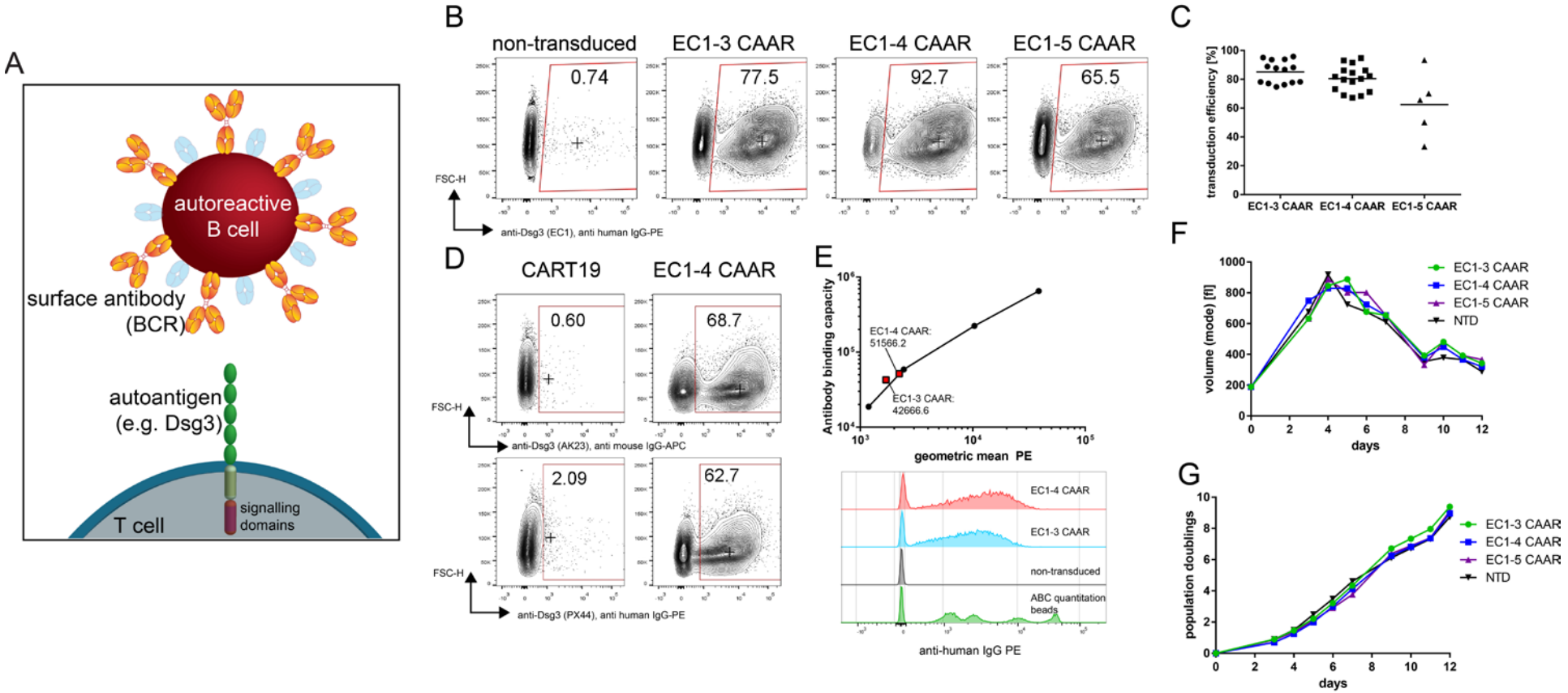

Fig. S1.

CAAR-T cells express high levels of conformational, mature Dsg3. (A) Schematic of the CAAR concept. (B) Surface staining of Dsg3 CAAR-T cells with anti-human Dsg3 EC1 (clone Px44) IgG. (C) Transduction efficiencies for each construct and experiment used throughout the studies; Dsg3EC1-3 and Dsg3EC1-4 CAAR show consistently robust expression in primary human T cells whereas Dsg3EC1-5 CAAR expression is variable. (D) Staining CART19 and Dsg3EC1-4 CAAR-T cells with AK23, which stains only mature conformational Dsg3, and Px44, which stains both conformational and denatured Dsg3, show comparable expression levels, indicating that the vast majority of the surface Dsg3 is native-like Dsg3. (E) CAAR surface expression level of a representative batch of EC1-3 and EC1-4 CAAR-T cells from the same normal human T cell donor indicates that Dsg3 CAAR T cells express 4-5e4 molecules per cell. CAAR surface expression levels are approximately half those observed with endogenous TCRs (10^5/cell (*55*)). CAAR-T cells were stained with anti-Dsg3 IgG (clone PVB28) which was detected with anti-human IgG PE (clone G18-145) at saturating concentrations. Antibody binding capacity was quantified by flow cytometry with calibrated anti-mouse IgG beads coated with saturating concentrations of G18-145-PE. Under saturating conditions, the fraction of monovalently binding IgGs represents the majority of bound antibodies. (F,G) Volume and proliferation of CAAR-T cells during expansion after stimulation with CD3/CD28 activating beads.

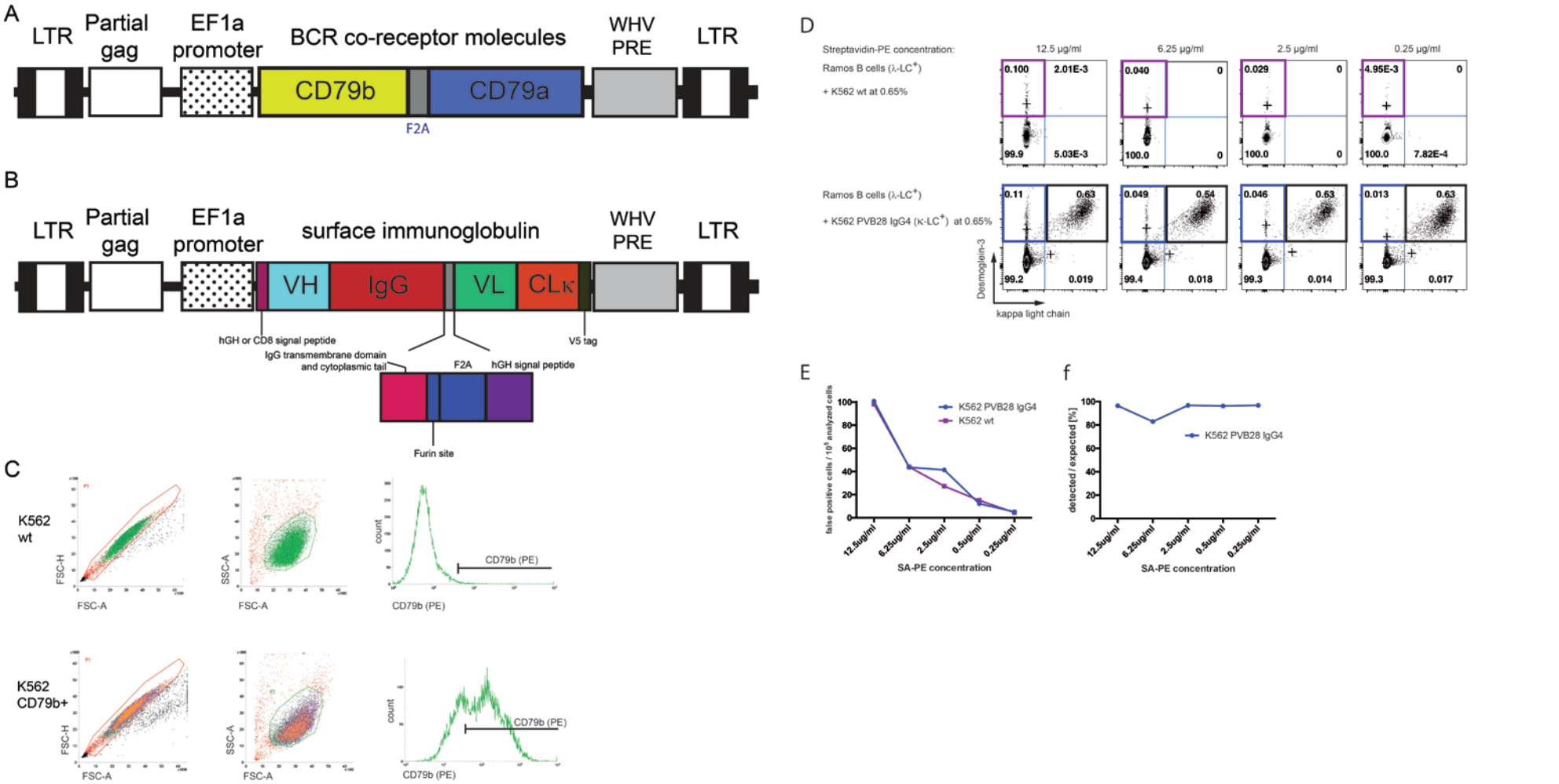

Fig. S2

Engineering and validation of target cells expressing anti-Dsg3 B cell receptors. Lentiviral constructs for expression of BCR surface immunoglobulin in K562 cells. (A) CD79a and CD79b were co-expressed from a lentiviral vector, separated by an F2A site. (B) Surface immunoglobulin was expressed as a single transcript, heavy chain and V5-tagged light chains separated by furin and F2A sites. Signal peptides from CD8 or human growth hormone (hGH) were used. (C) Sorting scheme for $CD79b^+$ K562 cells (BD influx). (D) To verify Dsg3-specific surface IgG staining, <1% K562 cells expressing PVB28 IgG4-kappa were mixed with Ramos B cells (expressing lambda light chain (LC)) and detected with anti-human kappa light chain and biotinylated Dsg3-Avitag. (E) Quantification of non-specific background and (F) Dsg3-specific staining indicates optimum streptavidin (SA)-PE concentration is 0.25 µg/mL. wt= wild type.

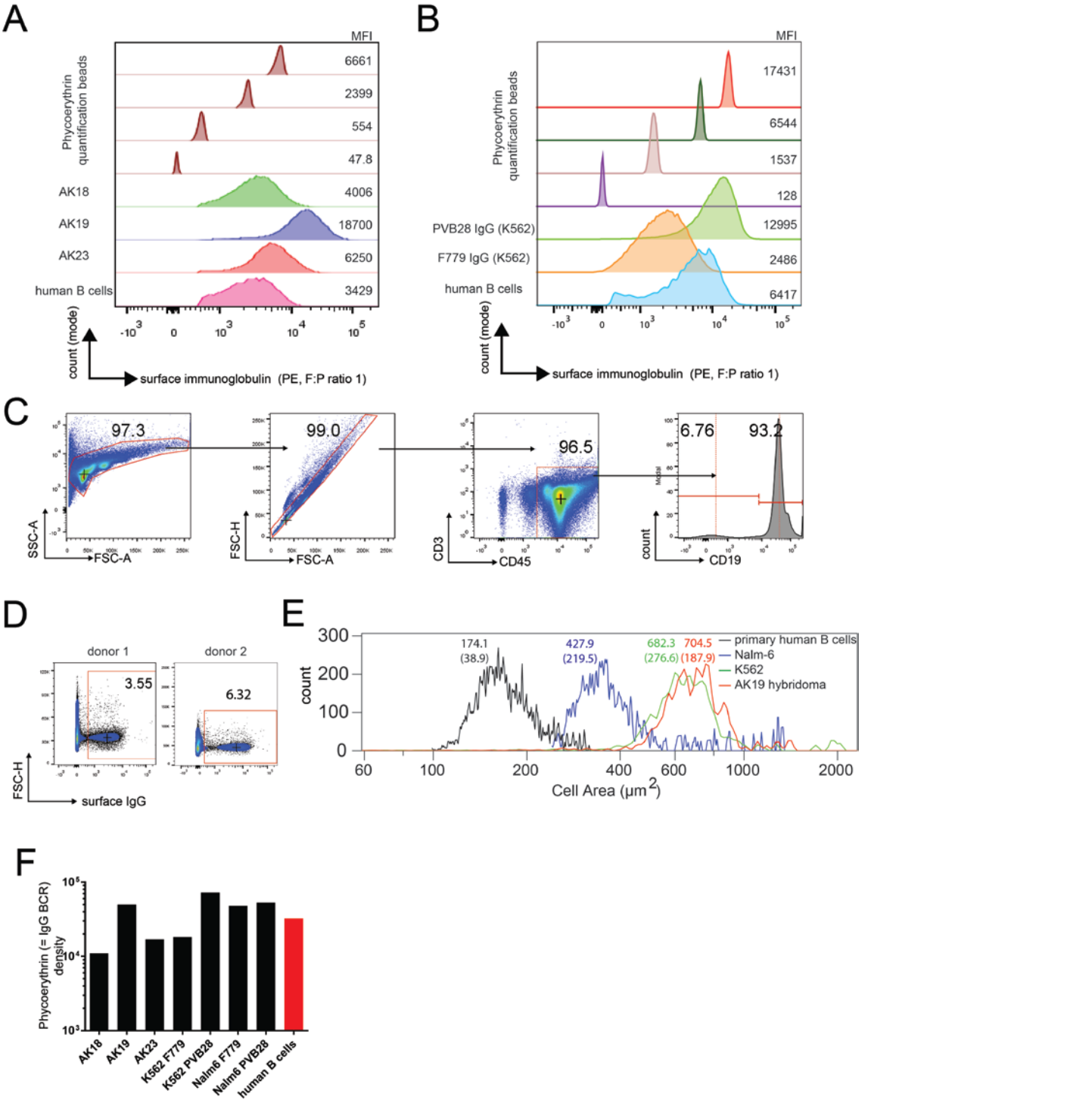

Fig. S3

Target cells express anti-Dsg3 BCRs at levels comparable to primary human IgG$^+$ B cells. (A,B) Histograms of phycoerythrin (PE) signal for PE quantification beads, target cells, and primary human B cells used for quantification of target cell surface BCRs (see Methods). F:P, fluorescence:protein. (C) Flow cytometric analysis of purified primary human B cells used for surface immunoglobulin expression analysis. (D) Anti-IgG PE plot of primary human B cells from which the histograms in A,B are derived. (E) Coulter counter histograms of cell surface area of primary human B cells compared to K562 and hybridoma cells. Mean cell surface area (standard deviation) is shown. (F) PE density, representing IgG BCR density, relative to a representative batch of primary human B cells from a healthy donor, indicates that all target cells express surface anti-Dsg3 BCRs at levels comparable to primary human IgG$^+$ B cells.

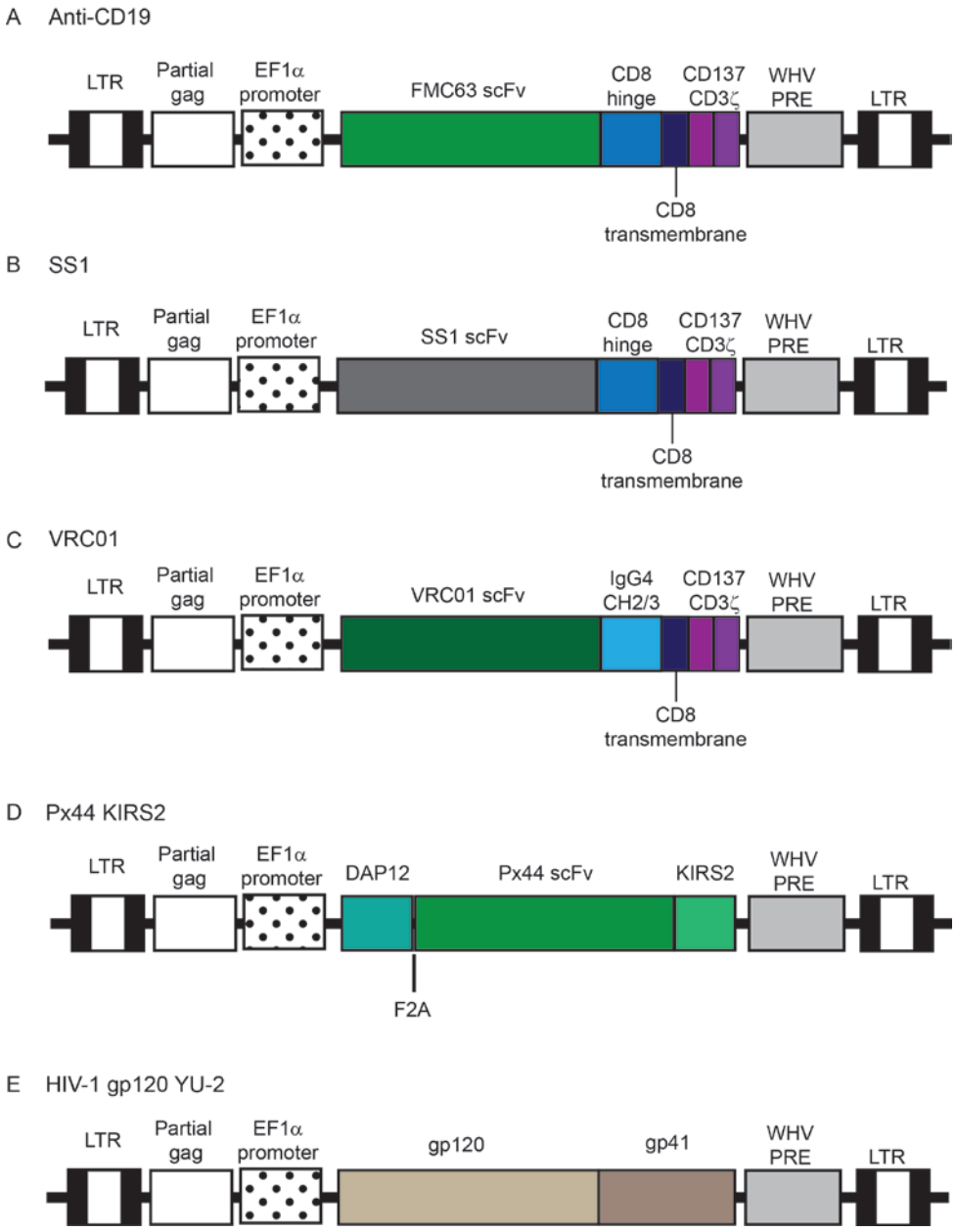

Fig. S4

Schematic of control CAR constructs. (A) Anti-CD19 (clone FMC63), negative control for PV hybridoma *in vitro* cytolysis and positive control for CD19^{+} Nalm6 *in vitro* cytolysis and *in vivo* model. (B) SS1, anti-mesothelin negative control in *in vitro* killing assays. (C) VRC01, anti-HIV-1 gp120 negative control in *in vitro* killing assays. (D) Px44, anti-Dsg3/1 positive control for *in vivo/in vitro* toxicity studies. (E) HIV-1 gp120/41 (isolate: YU-2) for expression on K562 cells, intended target for VRC01 CAR.

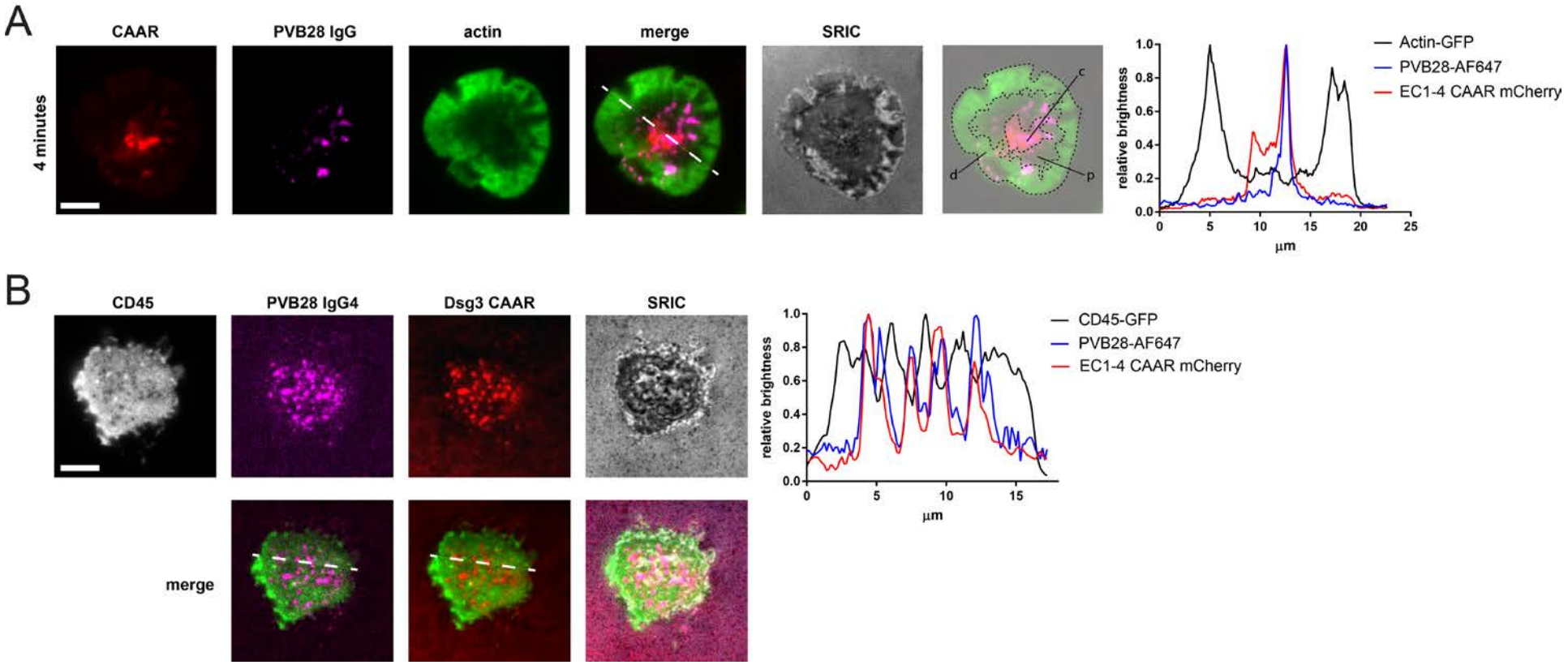

Fig. S5

TIRF microscopy of CAAR-BCR synapse formation. (A) TIRF microscopy demonstrates the Dsg3 CAAR forms immunologic synapses with central-c, peripheral-p, and distal-d supramolecular activation complexes mediated by actin cytoskeleton re-organization, and (B) relative CD45 exclusion from early CAAR-IgG microclusters (30 seconds after initial contact with the lipid bilayer). Graphs in (A) and (B) show localization of immunofluorescence intensity along dashed line. Scale bar=5 µm. SRIC= surface reflective interference contrast. Representative cells are shown and were confirmed in 3 independent experiments with observation of at least 20 cells per experiment.

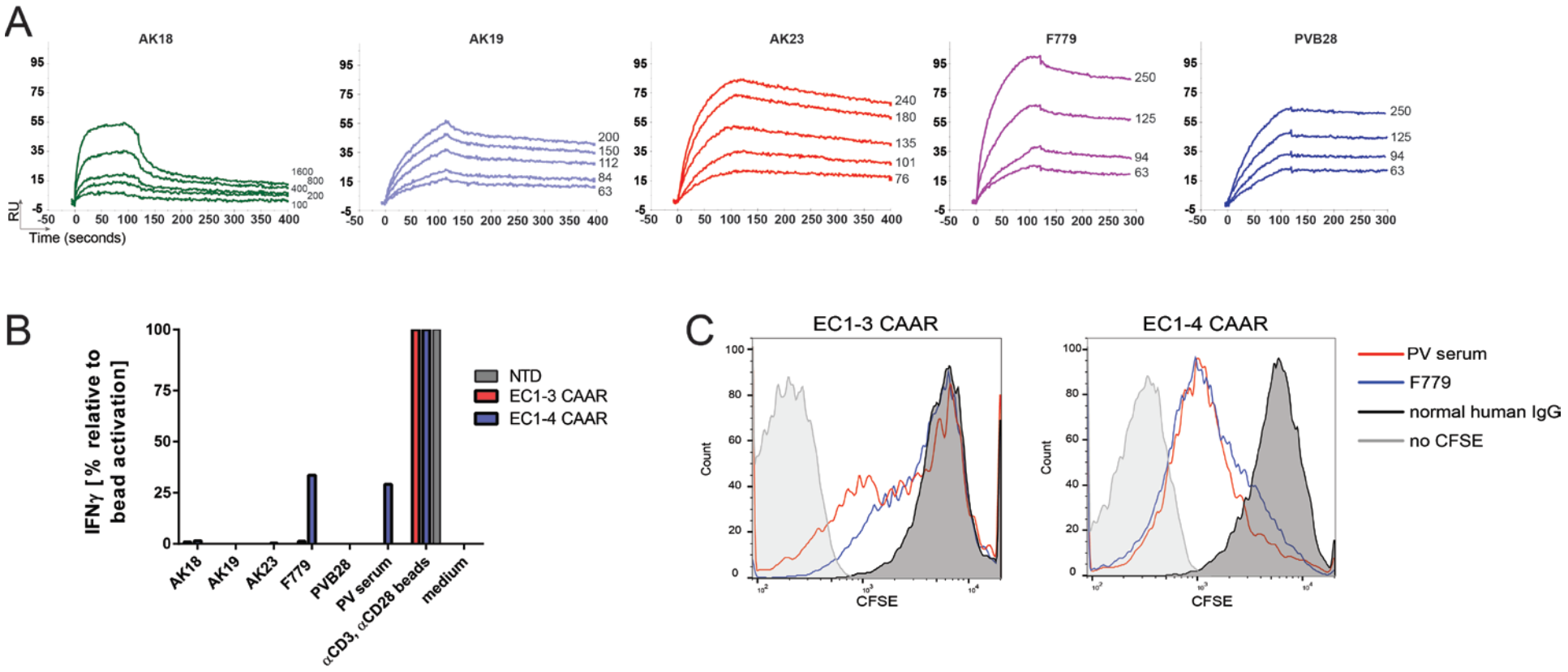

Fig. S6

Surface plasmon resonance analysis of anti-Dsg3 IgG binding kinetics. (A) Sensorgrams for binding of target IgGs to Dsg3 (concentrations in nM). Quantitative statistics shown in Fig. 2G and H indicate similar on-rates, but increased off-rates and lower affinity for non-inhibitory antibodies AK18, AK23, and F779. (B) Dsg3EC1-4 CAAR-Ts secrete IFNγ and (C) proliferate in response to F779 and PV serum IgG, more so than Dsg3EC1-3 CAAR-Ts, indicating low-level CAAR-T stimulation by anti-Dsg3 IgG. CAAR- T cells were incubated in the presence of 100µg/ml soluble monoclonal antibody or PV serum adjusted to a Dsg3 titer of 180IU/ml. Mean values of duplicate cultures are shown, data are representative of 3 independent experiments.

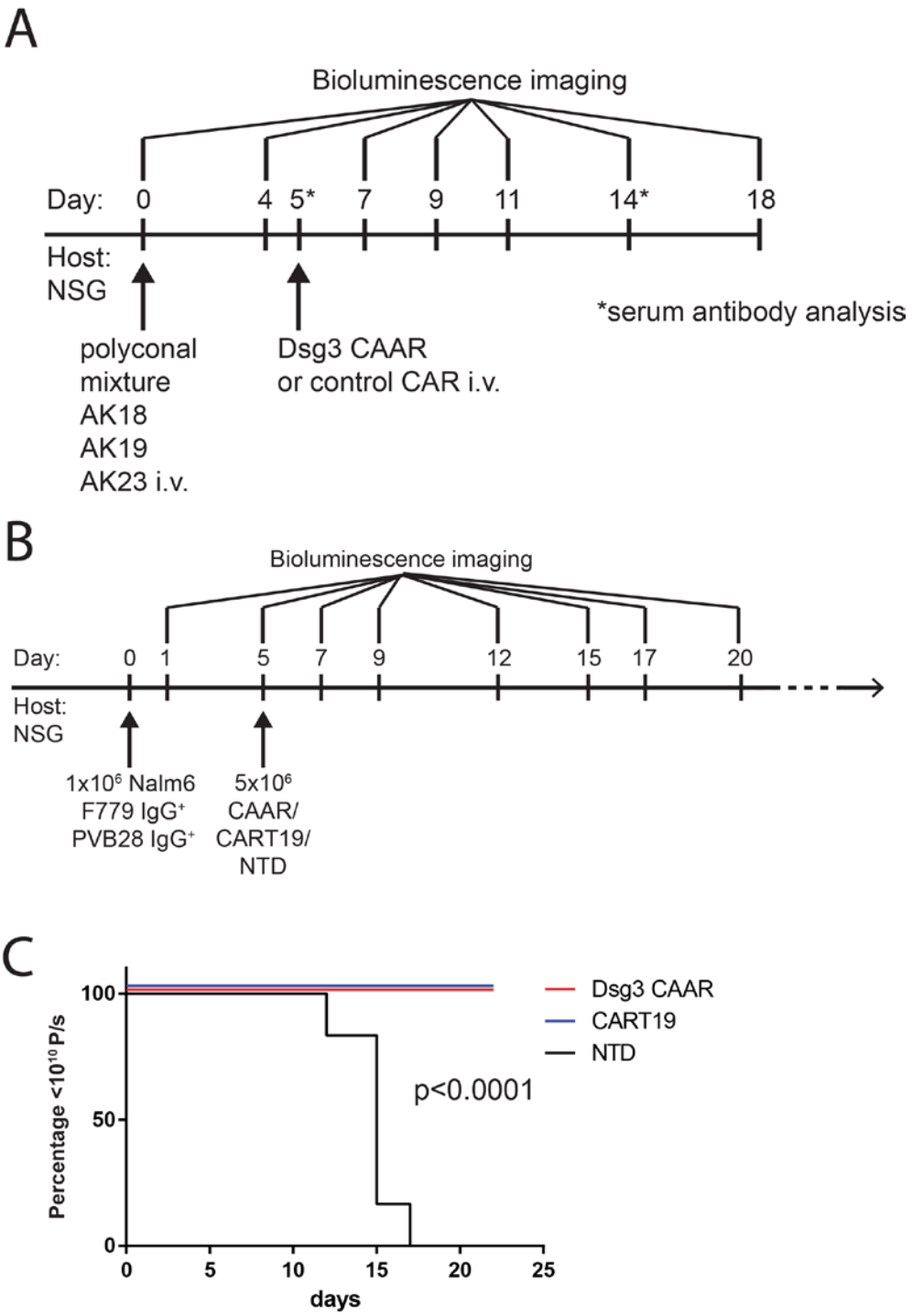

Fig. S7

Dsg3 CAAR-T cells eliminate anti-Dsg3 target cells *in vivo*. (A) Experimental design of the polyclonal antibody-secreting PV hybridoma model shown in Fig. 3A-D, with indicated injection time points, bioluminescence imaging and serum antibody analysis. (B) Experimental design for the human Nalm6 model expressing human sIg (F779 and PVB28) shown in Fig. 3E-H, with indicated injection time points and bioluminescence imaging. Mice were sacrificed 22 days after Nalm6 injection. (C) Kaplan-Meier curve for mice in the Nalm6 experiment reaching a bioluminescent signal of $>10^{10}$ photons/second (total flux). N=6 per group, log-rank (Mantel-Cox) test.

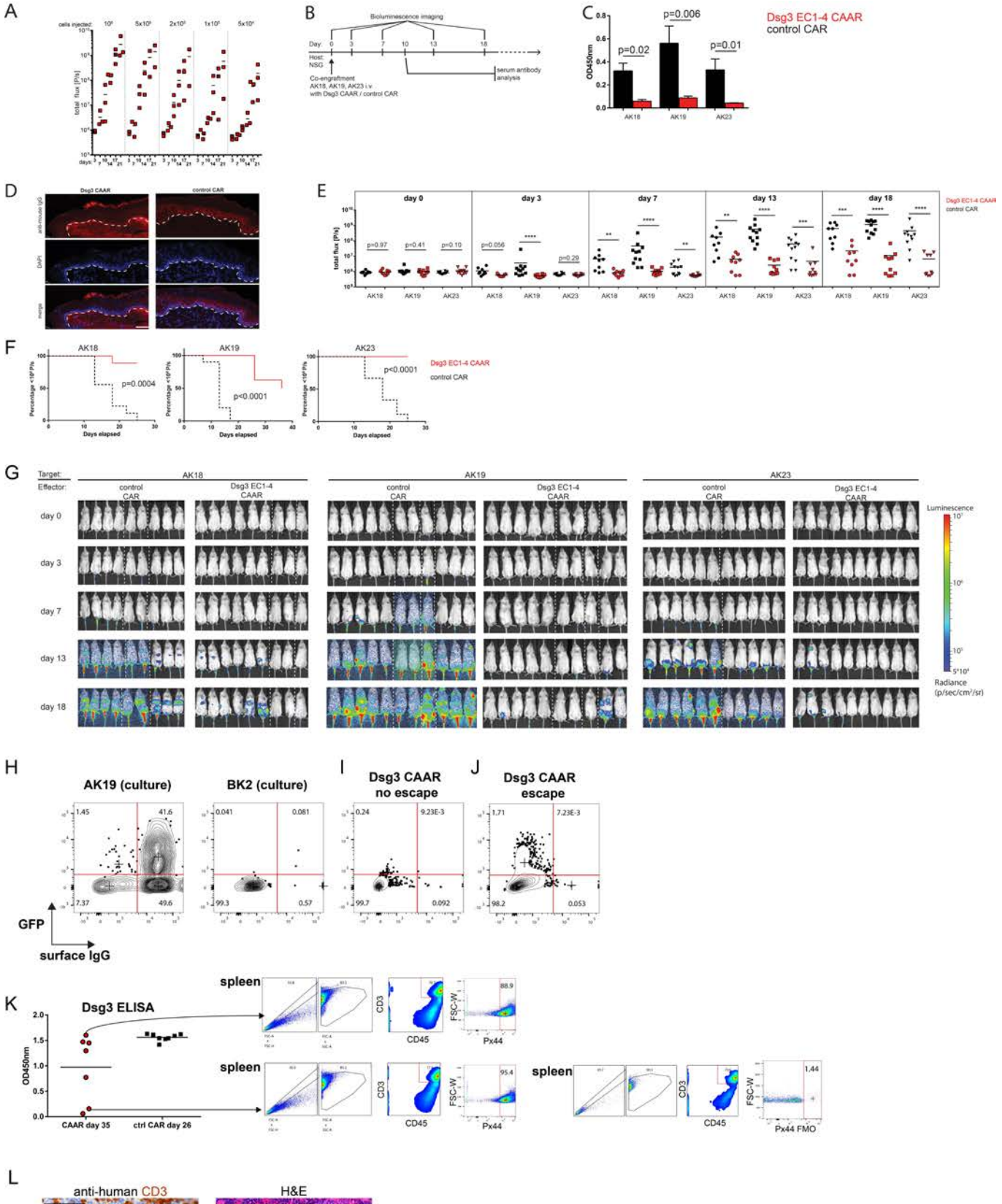
A
cells injected:
10⁶
5x10⁵
2x10⁵
1x10⁵
5x10⁴
total flux [P/s]
days
B
Bioluminescence imaging
Day:
Host:
NSG
Co-engraftment
AK18, AK19, AK23 i.v.
with Dsg3 CAAR / control CAR
serum antibody analysis
C
p=0.006
p=0.02
p=0.01
OD450nm
AK18
AK19
AK23
Dsg3 EC1-4 CAAR
control CAR
D
Dsg3 CAAR
control CAR
anti-mouse IgG
DAPI
merge
E
day 0
day 3
day 7
day 13
day 18
total flux [P/s]
p=0.97
p=0.41
p=0.10
p=0.056
p=0.29
Dsg3 EC1-4 CAAR
control CAR
F
AK18
AK19
AK23
p=0.0004
p<0.0001
p<0.0001
Percentage <10⁶ P/s
Days elapsed
Dsg3 EC1-4 CAAR
control CAR
G
Target:
Effector:
AK18
AK19
AK23
control CAR
Dsg3 EC1-4 CAAR
day 0
day 3
day 7
day 13
day 18
Luminescence
Radiance (p/sec/cm²/sr)
H
AK19 (culture)
BK2 (culture)
1.45
41.6
7.37
49.6
0.041
0.081
99.3
0.57
GFP
surface IgG
I
Dsg3 CAAR no escape
0.24
9.23E-3
99.7
0.092
J
Dsg3 CAAR escape
1.71
7.23E-3
98.2
0.053
K
Dsg3 ELISA
OD450nm
CAAR day 35
ctrl CAR day 26
spleen
CD3
CD45
FSC-W
Px44
88.9
95.4
1.44
Px44 FMO
L
anti-human CD3
H&E

Fig. S8

Fig. S8

Dsg3EC1-4 CAAR-T cells control antibody-secreting sIg$^+$ but not sIg$^-$ PV hybridoma cells and persist despite presence of soluble anti-Dsg3 antibodies. (A) Different numbers of AK23 expressing click-beetle red luciferase/GFP were injected intravenously into NSG mice and bioluminescence was assessed at indicated time points. Doubling time *in vivo* is approximately 24 hours once a total flux of $5x10^6$ photons/s is reached. (B) Experimental design for antibody-secreting PV hybridoma model. (C) Reduced serum anti-Dsg3 ELISA reflects hybridoma control in CAAR-T-treated mice. (D) Negative mucosa direct immunofluorescence reflects hybridoma control in CAAR-T-treated mice. Scale bar=50 μm. (E) Serial quantification of hybridoma burden by bioluminescence imaging. (F) Kaplan-Meier curves for CAAR-T-treated mice using a 100-fold hybridoma expansion (total flux $>10^8$ photons/s) as an endpoint representing lack of disease control. (G) Serial quantification of hybridoma burden by bioluminescence imaging. White dashed lines separate images from different cages/experiments. (H) Representative flow cytometric analysis of sIg expression in AK19 (GFP$^+$) and BK2 (surface IgG$^-$, GFP$^-$) hybridoma cells in culture, indicating that approximately 1% of AK19 cells are sIg$^-$. (I) Flow cytometric analysis of the bone marrow of Dsg3-CAAR treated mice with no bioluminescence signal at day 18 (no escape) shows that no significant GFP+ populations are detectable. (J) Escape from Dsg3EC1-4 CAAR T cell control is caused by GFP$^+$ sIgG$^-$ hybridoma cells. (K) Mice challenged with AK19 were treated with Dsg3EC1-4 CAAR-T or control CAR-T cells and allowed to progress for an extended period of time. In a fraction of CAAR-treated mice, serum anti-Dsg3 antibodies were detectable (due to escape as shown in E-G). Spleens of these mice were harvested and CAAR-T cells were detectable in all mice at comparable frequencies by flow cytometry, indicating that lack of CAAR-T cell persistence or loss of Dsg3 CAAR expression on T cells is not responsible for Dsg3 CAAR escape. Representative plots are shown from 2 mice and the fluorescence-minus-one (FMO) control, which was stained with the same antibody cocktail except for anti-Dsg3 (Px44-AF647). (L) Representative spleen sample showing engraftment and persistence of CAAR-Ts even in the absence of Dsg3-BCR expressing target cells (scale bar =100 μm).

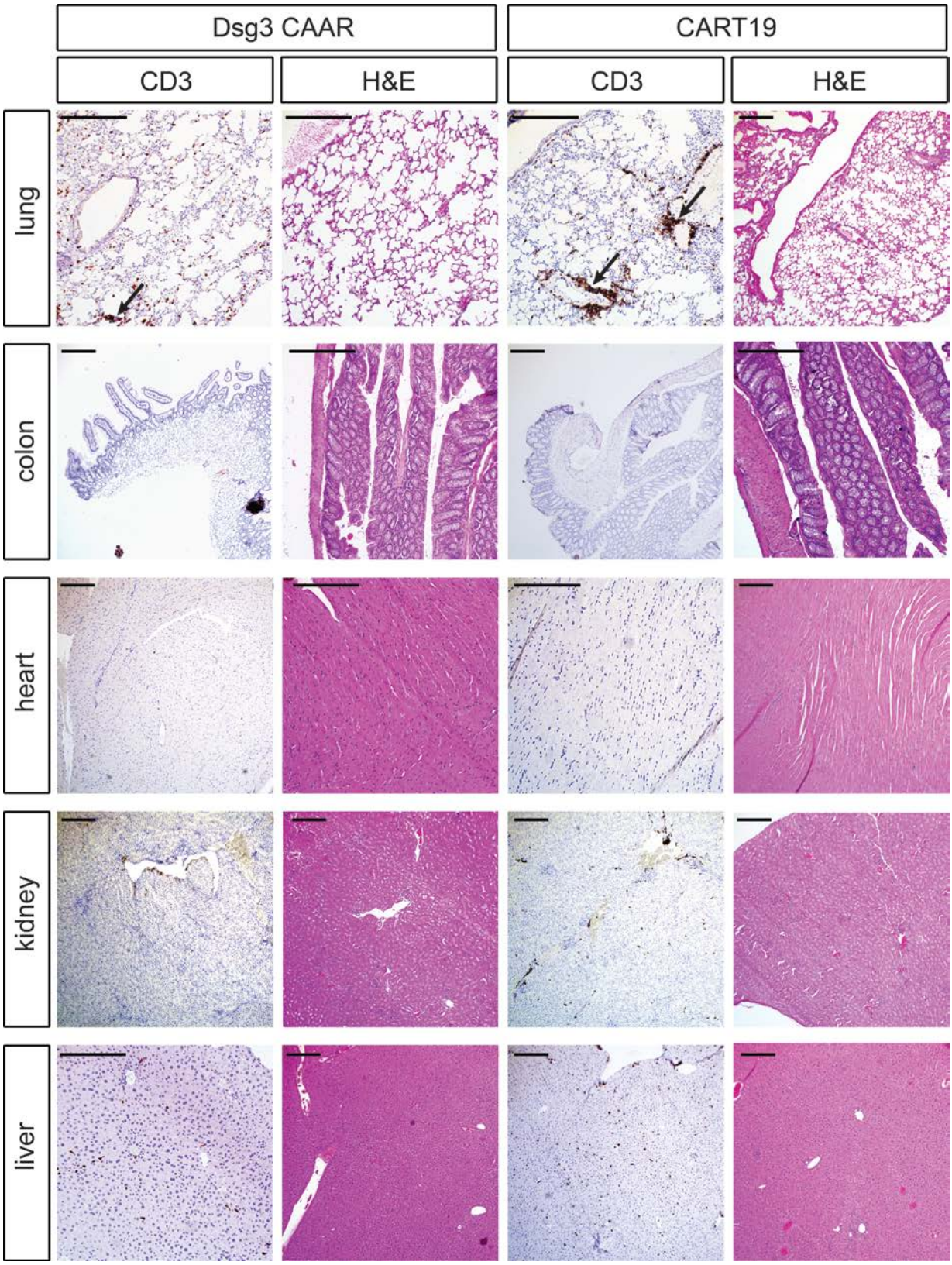

Fig. S9

No off-target toxicity against desmosome-bearing murine lung, gut, heart, liver, and kidney by CAAR-T cells. 1-2x10^6 Dsg3 CAAR-T or CART19 cells from one healthy human donor (n=3 per group) were engrafted into NSG mice that were sacrificed 18 days later; indicated organs were harvested, H&E stained and subjected to immunohistochemistry for human $CD3^+$ CAAR-T detection. Mild T cell infiltration into lung tissue was observed in Dsg3 CAAR and CART19 treated mice (arrows) and was interpreted as early xenoreactive graft versus host disease, which is expected in this experimental model. Scale bars = 125 μm.

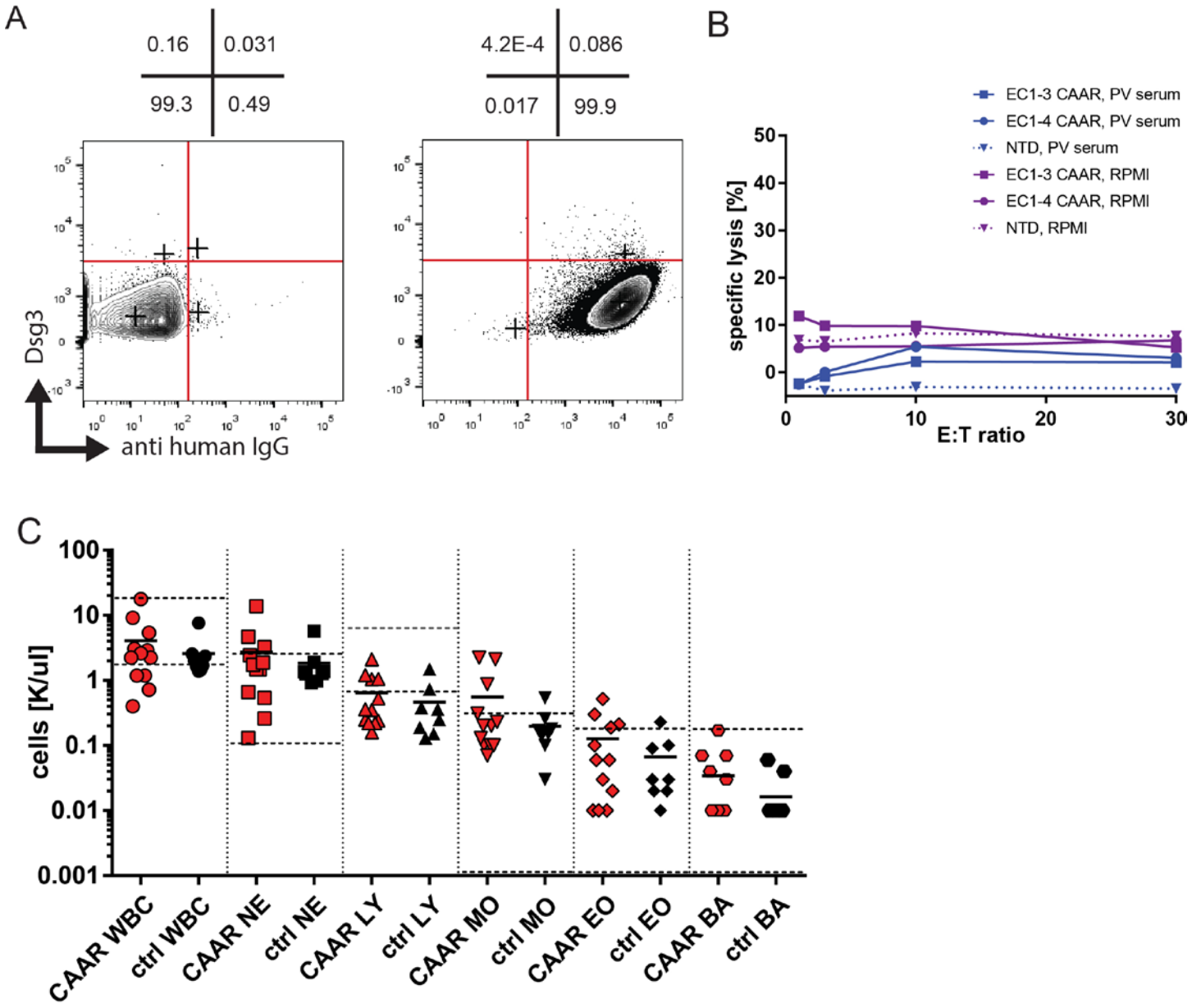

Fig. S10

Dsg3 CAAR-T cells do not show off-target toxicity. (A) $CD64^{+}$(FcγRI)K562 cells were loaded with PV serum IgG and sIg binding was confirmed by flow cytometry. (B) ^{51}Cr- release into supernatant was measured after 4 hours of co-culture of loaded target cells and CAAR-T cells. Mean values of triplicate culture are shown; data are representative of 2 independent experiments. (C) Differential blood count of Dsg3 CAAR-T-treated mice confirms lack of cytotoxicity against Fcγ-receptor-expressing cells *in vivo*. K/μl=thousand cells per microliter. Dashed lines indicate normal range. Black horizontal lines indicate the mean of each group. WBC: white blood count; NE: neutrophils; LY: lymphocytes; MO: monocytes; EO: eosinophils, BA: basophils. Data are pooled from 2 independent experiments. No significant difference was detected for any of the cell types in any of the experiments. T-test, 2-tailed.

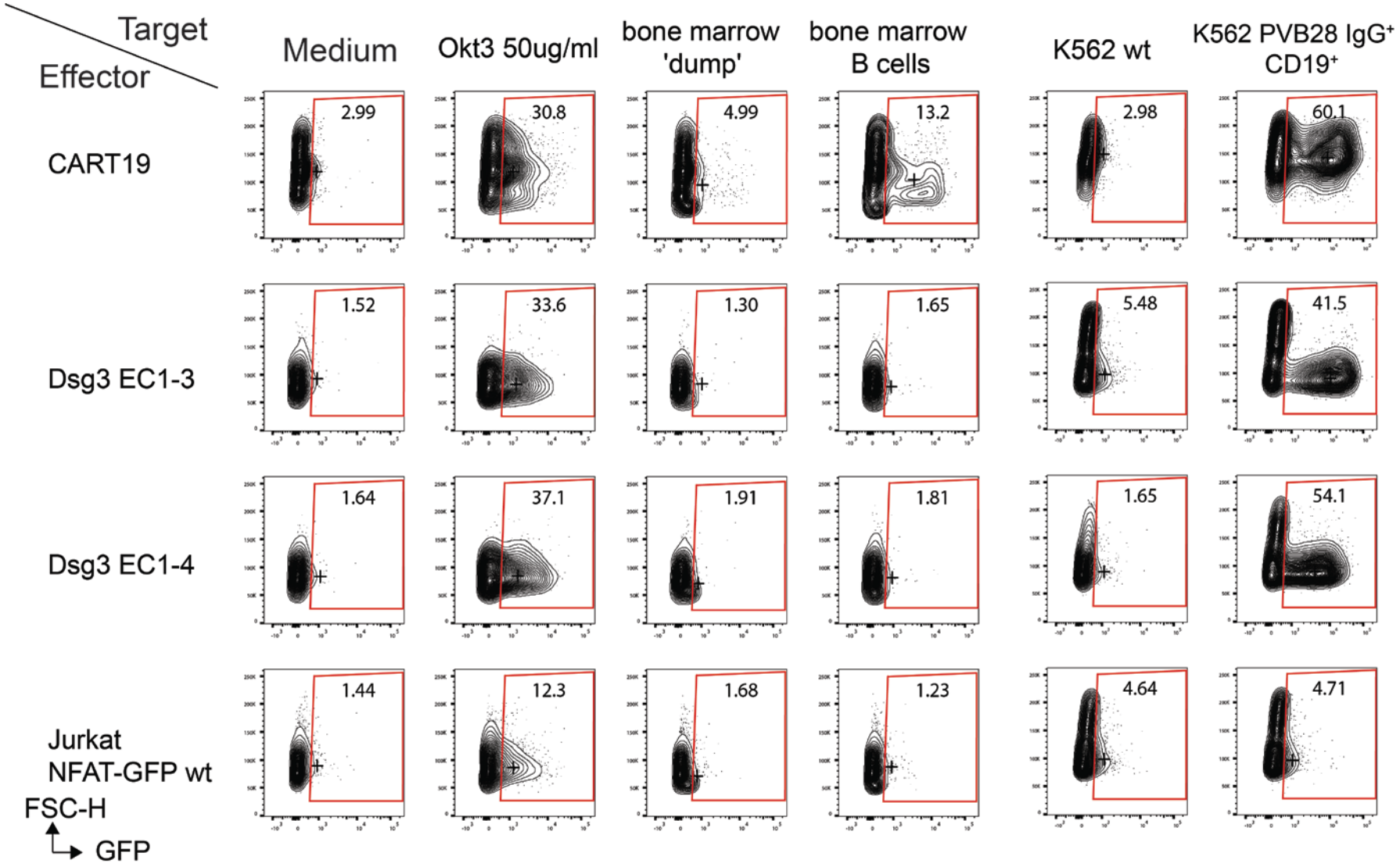

Fig. S11

Immature bone marrow B cells are not subject to off-target toxicity. Jurkat NFAT-GFP Dsg3 CAAR-T cells do not show signaling in response to immature $CD20^+$ bone marrow B cells, indicating that theoretical targeting of polyreactive or potentially Dsg3-autoreactive immature B cells in the bone marrow will not cause significant toxicity. Wildtype (wt) NFAT-GFP Jurkat cells or those expressing Dsg3EC1-3/EC1-4 CAARs or CD19 CAR were incubated for 16 hours with indicated target cells and their GFP expression was assessed by flow cytometry. Okt3, positive control for activating NFAT-GFP signaling. K562 PVB28 IgG^+ $CD19^+$ cells, positive control for activation of CART19 and Dsg3 CAAR signaling. Numbers represent the percentage of GFP positive cells. Crosses represent the MFI of the GFP positive population.

Table S1. Primers for construction of the Dsg3 CAAR.

Fragment	Template	Primer (F=forward, R=reverse)	Cloning Notes
EF1 alpha promoter	human PBMC genomic DNA	F: 5'GGATCCTGCTAGACTCACGACACCTGAAATGGAAG	adds Kozak sequence and BamHI site
		R: 5' GAGGAGGTCGACATTCGTGAGGCTCCGGTGCCCGTC	overlap to the propeptide sequence of Dsg3
Human Dsg3 EC1-5	GeneArt	F: 5'GAGGAGGAGGGATCCGCCACC	Gene fragment includes BamHI, CD8 signal peptide, Dsg3 EC1-5; CD8 hinge replaced with GS linker and NheI site
		R: 5'CCTCCGCCGCCGCTAGCTCTGCC	
Human Dsg3 EC1-4	GeneArt	F: 5'GAGGAGGAGGGATCCGCCACC	Gene fragment includes BamHI, CD8 signal peptide, Dsg3 EC1-4; CD8 hinge replaced with GS linker and NheI site
		R: 5'CCTCCGCCGCCGCTAGCCTTTTCCAGCACGGCGG	
Human Dsg3 EC1-3	GeneArt	F: 5'GAGGAGGAGGGATCCGCCACC	Gene fragment includes BamHI, CD8 signal peptide, Dsg3 EC1-3; CD8 hinge replaced with GS linker and NheI site
		R: 5'TCTCCTCGCTAGCGAAGGCAATGCCC	
CD8 hinge and transmembrane region	human PBMC cDNA	F: 5'CTCAGGGAGGAAGCCCACCACGACGCCAGCGCCGC	overlap to EC5 of human Dsg3
		R: 5'CCCCGTTTGGTGATAACCAGTGACAGGAGAAGG	overlap to human CD137 signal transduction domain
CD137 signal transduction domain	human PBMC cDNA	F: 5'CTGGTTATCACCAAACGGGGCAGAAAGAAACTCC	
		R: 5'TTCACTCTCAGTTCACATCCTCCTTCTTCTTCTTCTGG	overlap to human CD3 zeta signal transduction domain
CD3 zeta signal transduction domain	human PBMC cDNA	F: 5'GATGTGAACTGAGAGTGAAGTTCAGCAGGAGCGC	
		R: 5' GGTTGATTGTCGACGCGGATCTTAGCGAGGGGGC	adds SalI site after TAA stop codon

Movie 1: CAAR synapse formation as observed by TIRF microscopy is associated with actin reorganization and centripetal movement of CAAR-sIg complexes. Jurkat T cells were transduced with actin-GFP and a Dsg3EC1-4 CAAR that was tagged with mCherry at the C-terminus of the cytoplasmic tail. Planar lipid bilayers were loaded with ICAM-1 (unlabeled) and PVB28 IgG4-AF647 at a density of ~250 molecules/μm^2. CAAR-T cells were allowed to react with the target molecules on the lipid bilayer at 37^oC and images in the GFP, mCherry, AF647 channels and the SRIC mode were acquired every 3 seconds. Channels were computationally overlaid. Scale bar = 10μm.

Movie 2: CD45 is excluded from early Dsg3 CAAR-sIg microclusters and enriched in the periphery of the immunologic synapse. Jurkat T cells were transduced with CD45-GFP and Dsg3EC1-4 CAAR-mCherry. Planar lipid bilayers were loaded with ICAM-1 (unlabeled) and PVB28 IgG4-AF647 at a density of ~250 molecules/μm^2. CAAR T cells were allowed to react with the target molecules on the lipid bilayer at 37^oC and images in the GFP, mCherry, AF647 channels and the SRIC mode were acquired every 3 seconds. Channels were computationally overlaid. Scale bar = 10μm.

Full Reference List

1. A. S. Payne, J. R. Stanley, in *Dermatology in General Medicine*, K. Wolff *et al.*, Eds. (McGraw Hill, New York, 2012), chap. 53.

2. N. Colliou, D. Picard, F. Caillot, S. Calbo, S. Le Corre, A. Lim, B. Lemercier, B. Le Mauff, M. Maho-Vaillant, S. Jacquot, C. Bedane, P. Bernard, F. Caux, C. Prost, E. Delaporte, M. S. Doutre, B. Dreno, N. Franck, S. Ingen-Housz-Oro, O. Chosidow, C. Pauwels, C. Picard, J. C. Roujeau, M. Sigal, E. Tancrede-Bohin, I. Templier, R. Eming, M. Hertl, M. D'Incan, P. Joly, P. Musette, Long-term remissions of severe pemphigus after rituximab therapy are associated with prolonged failure of desmoglein B cell response. *Sci. Transl. Med.* **5**, 175ra30 (2013). Medline doi:10.1126/scitranslmed.3005166

3. R. Eming, A. Nagel, S. Wolff-Franke, E. Podstawa, D. Debus, M. Hertl, Rituximab exerts a dual effect in pemphigus vulgaris. *J. Invest. Dermatol.* **128**, 2850–2858 (2008). Medline doi:10.1038/jid.2008.172

4. L. Lunardon, K. J. Tsai, K. J. Propert, N. Fett, J. R. Stanley, V. P. Werth, D. E. Tsai, A. S. Payne, Adjuvant rituximab therapy of pemphigus: A single-center experience with 31 patients. *Arch. Dermatol.* **148**, 1031–1036 (2012). Medline doi:10.1001/archdermatol.2012.1522

5. C. M. Hammers, J. Chen, C. Lin, S. Kacir, D. L. Siegel, A. S. Payne, J. R. Stanley, Persistence of anti-desmoglein 3 IgG^+ B-cell clones in pemphigus patients over years. *J. Invest. Dermatol.* **135**, 742–749 (2015). Medline doi:10.1038/jid.2014.291

6. D. L. Porter, B. L. Levine, M. Kalos, A. Bagg, C. H. June, Chimeric antigen receptor-modified T cells in chronic lymphoid leukemia. *N. Engl. J. Med.* **365**, 725–733 (2011). Medline doi:10.1056/NEJMoa1103849

7. S. L. Maude, N. Frey, P. A. Shaw, R. Aplenc, D. M. Barrett, N. J. Bunin, A. Chew, V. E. Gonzalez, Z. Zheng, S. F. Lacey, Y. D. Mahnke, J. J. Melenhorst, S. R. Rheingold, A. Shen, D. T. Teachey, B. L. Levine, C. H. June, D. L. Porter, S. A. Grupp, Chimeric antigen receptor T cells for sustained remissions in leukemia. *N. Engl. J. Med.* **371**, 1507–1517 (2014). Medline doi:10.1056/NEJMoa1407222

8. M. L. Davila, I. Riviere, X. Wang, S. Bartido, J. Park, K. Curran, S. S. Chung, J. Stefanski, O. Borquez-Ojeda, M. Olszewska, J. Qu, T. Wasielewska, Q. He, M. Fink, H. Shinglot, M. Youssif, M. Satter, Y. Wang, J. Hosey, H. Quintanilla, E. Halton, Y. Bernal, D. C. Bouhassira, M. E. Arcila, M. Gonen, G. J. Roboz, P. Maslak, D. Douer, M. G. Frattini, S. Giralt, M. Sadelain, R. Brentjens, Efficacy and toxicity management of 19-28z CAR T cell therapy in B cell acute lymphoblastic leukemia. *Sci. Transl. Med.* **6**, 224ra25 (2014). Medline

9. D. W. Lee, J. N. Kochenderfer, M. Stetler-Stevenson, Y. K. Cui, C. Delbrook, S. A. Feldman, T. J. Fry, R. Orentas, M. Sabatino, N. N. Shah, S. M. Steinberg, D. Stroncek, N. Tschernia, C. Yuan, H. Zhang, L. Zhang, S. A. Rosenberg, A. S. Wayne, C. L. Mackall, T cells expressing CD19 chimeric antigen receptors for acute lymphoblastic leukaemia in children and young adults: A phase 1 dose-escalation trial. *Lancet* **385**, 517–528 (2015). Medline doi:10.1016/S0140-6736(14)61403-3

10. J. N. Kochenderfer, M. E. Dudley, S. H. Kassim, R. P. Somerville, R. O. Carpenter, M. Stetler-Stevenson, J. C. Yang, G. Q. Phan, M. S. Hughes, R. M. Sherry, M. Raffeld, S. Feldman, L. Lu, Y. F. Li, L. T. Ngo, A. Goy, T. Feldman, D. E. Spaner, M. L. Wang, C. C. Chen, S. M. Kranick, A. Nath, D. A. Nathan, K. E. Morton, M. A. Toomey, S. A. Rosenberg, Chemotherapy-refractory diffuse large B-cell lymphoma and indolent B-cell malignancies can be effectively treated with autologous T cells expressing an anti-CD19 chimeric antigen receptor. *J. Clin. Oncol.* **33**, 540–549 (2015). Medline doi:10.1200/JCO.2014.56.2025

11. R. J. Brentjens, I. Rivière, J. H. Park, M. L. Davila, X. Wang, J. Stefanski, C. Taylor, R. Yeh, S. Bartido, O. Borquez-Ojeda, M. Olszewska, Y. Bernal, H. Pegram, M. Przybylowski, D. Hollyman, Y. Usachenko, D. Pirraglia, J. Hosey, E. Santos, E. Halton, P. Maslak, D. Scheinberg, J. Jurcic, M. Heaney, G. Heller, M. Frattini, M. Sadelain, Safety and persistence of adoptively transferred autologous CD19-targeted T cells in patients with relapsed or chemotherapy refractory B-cell leukemias. *Blood* **118**, 4817–4828 (2011). Medline

12. C. R. Cruz, K. P. Micklethwaite, B. Savoldo, C. A. Ramos, S. Lam, S. Ku, O. Diouf, E. Liu, A. J. Barrett, S. Ito, E. J. Shpall, R. A. Krance, R. T. Kamble, G. Carrum, C. M. Hosing, A. P. Gee, Z. Mei, B. J. Grilley, H. E. Heslop, C. M. Rooney, M. K. Brenner, C. M. Bollard, G. Dotti, Infusion of donor-derived CD19-redirected virus-specific T cells for B-cell malignancies relapsed after allogeneic stem cell transplant: A phase 1 study. *Blood* **122**, 2965–2973 (2013). Medline doi:10.1182/blood-2013-06-506741

13. B. Savoldo, C. A. Ramos, E. Liu, M. P. Mims, M. J. Keating, G. Carrum, R. T. Kamble, C. M. Bollard, A. P. Gee, Z. Mei, H. Liu, B. Grilley, C. M. Rooney, H. E. Heslop, M. K. Brenner, G. Dotti, CD28 costimulation improves expansion and persistence of chimeric antigen receptor-modified T cells in lymphoma patients. *J. Clin. Invest.* **121**, 1822–1826 (2011). Medline doi:10.1172/JCI46110

14. C. J. Turtle, L. A. Hanafi, C. Berger, T. A. Gooley, S. Cherian, M. Hudecek, D. Sommermeyer, K. Melville, B. Pender, T. M. Budiarto, E. Robinson, N. N. Steevens, C. Chaney, L. Soma, X. Chen, C. Yeung, B. Wood, D. Li, J. Cao, S. Heimfeld, M. C. Jensen, S. R. Riddell, D. G. Maloney, CD19 CAR-T cells of defined $CD4^+$:$CD8^+$ composition in adult B cell ALL patients. *J. Clin. Invest.* **126**, 2123–2138 (2016). Medline doi:10.1172/JCI85309

15. A. Al-Amoudi, D. C. Díez, M. J. Betts, A. S. Frangakis, The molecular architecture of cadherins in native epidermal desmosomes. *Nature* **450**, 832–837 (2007). Medline doi:10.1038/nature05994

16. B. Ohyama, K. Nishifuji, P. T. Chan, A. Kawaguchi, T. Yamashita, N. Ishii, T. Hamada, T. Dainichi, H. Koga, D. Tsuruta, M. Amagai, T. Hashimoto, Epitope spreading is rarely found in pemphigus vulgaris by large-scale longitudinal study using desmoglein 2-based swapped molecules. *J. Invest. Dermatol.* **132**, 1158–1168 (2012). Medline doi:10.1038/jid.2011.448

17. K. Choudhuri, D. Wiseman, M. H. Brown, K. Gould, P. A. van der Merwe, T-cell receptor triggering is critically dependent on the dimensions of its peptide-MHC ligand. *Nature* **436**, 578–582 (2005). Medline doi:10.1038/nature03843

18. S. Hennecke, P. Cosson, Role of transmembrane domains in assembly and intracellular transport of the CD8 molecule. *J. Biol. Chem.* **268**, 26607–26612 (1993). Medline

19. K. Tsunoda, T. Ota, M. Aoki, T. Yamada, T. Nagai, T. Nakagawa, S. Koyasu, T. Nishikawa, M. Amagai, Induction of pemphigus phenotype by a mouse monoclonal antibody against the amino-terminal adhesive interface of desmoglein 3. *J. Immunol.* **170**, 2170–2178 (2003). Medline doi:10.4049/jimmunol.170.4.2170

20. G. Di Zenzo, G. Di Lullo, D. Corti, V. Calabresi, A. Sinistro, F. Vanzetta, B. Didona, G. Cianchini, M. Hertl, R. Eming, M. Amagai, B. Ohyama, T. Hashimoto, J. Sloostra, F. Sallusto, G. Zambruno, A. Lanzavecchia, Pemphigus autoantibodies generated through somatic mutations target the desmoglein-3 cis-interface. *J. Clin. Invest.* **122**, 3781–3790 (2012). Medline doi:10.1172/JCI64413

21. M. J. Cho, A. S. Lo, X. Mao, A. R. Nagler, C. T. Ellebrecht, E. M. Mukherjee, C. M. Hammers, E. J. Choi, P. M. Sharma, M. Uduman, H. Li, A. H. Rux, S. A. Farber, C. B. Rubin, S. H. Kleinstein, B. S. Sachais, M. R. Posner, L. A. Cavacini, A. S. Payne, Shared VH1-46 gene usage by pemphigus vulgaris autoantibodies indicates common humoral immune responses among patients. *Nat. Commun.* **5**, 4167 (2014). Medline doi:10.1038/ncomms5167

22. C. R. F. Monks, B. A. Freiberg, H. Kupfer, N. Sciaky, A. Kupfer, Three-dimensional segregation of supramolecular activation clusters in T cells. *Nature* **395**, 82–86 (1998). Medline doi:10.1038/25764

23. A. Grakoui, S. K. Bromley, C. Sumen, M. M. Davis, A. S. Shaw, P. M. Allen, M. L. Dustin, The immunological synapse: A molecular machine controlling T cell activation. *Science* **285**, 221–227 (1999). Medline doi:10.1126/science.285.5425.221

24. J. R. James, R. D. Vale, Biophysical mechanism of T-cell receptor triggering in a reconstituted system. *Nature* **487**, 64–69 (2012). Medline

25. R. Varma, G. Campi, T. Yokosuka, T. Saito, M. L. Dustin, T cell receptor-proximal signals are sustained in peripheral microclusters and terminated in the central supramolecular activation cluster. *Immunity* **25**, 117–127 (2006). Medline doi:10.1016/j.immuni.2006.04.010

26. S. J. Davis, P. A. van der Merwe, The kinetic-segregation model: TCR triggering and beyond. *Nat. Immunol.* **7**, 803–809 (2006). Medline doi:10.1038/ni1369

27. I. Melero, W. W. Shuford, S. A. Newby, A. Aruffo, J. A. Ledbetter, K. E. Hellström, R. S. Mittler, L. Chen, Monoclonal antibodies against the 4-1BB T-cell activation molecule eradicate established tumors. *Nat. Med.* **3**, 682–685 (1997). Medline doi:10.1038/nm0697-682

28. Z. Ye, I. Hellström, M. Hayden-Ledbetter, A. Dahlin, J. A. Ledbetter, K. E. Hellström, Gene therapy for cancer using single-chain Fv fragments specific for 4-1BB. *Nat. Med.* **8**, 343–348 (2002). Medline doi:10.1038/nm0402-343

29. S. Yang, Y. Yang, J. Raycraft, H. Zhang, S. Kanan, Y. Guo, Z. Ronai, I. Hellstrom, K. E. Hellstrom, Melanoma cells transfected to express CD83 induce antitumor immunity that can be increased by also engaging CD137. *Proc. Natl. Acad. Sci. U.S.A.* **101**, 4990–4995 (2004). Medline doi:10.1073/pnas.0400880101

30. Z. Zhao, M. Condomines, S. J. van der Stegen, F. Perna, C. C. Kloss, G. Gunset, J. Plotkin, M. Sadelain, Structural design of engineered costimulation determines tumor rejection kinetics and persistence of CAR T cells. *Cancer Cell* **28**, 415–428 (2015). Medline

31. A. H. Long, W. M. Haso, J. F. Shern, K. M. Wanhainen, M. Murgai, M. Ingaramo, J. P. Smith, A. J. Walker, M. E. Kohler, V. R. Venkateshwara, R. N. Kaplan, G. H. Patterson, T. J. Fry, R. J. Orentas, C. L. Mackall, 4-1BB costimulation ameliorates T cell exhaustion induced by tonic signaling of chimeric antigen receptors. *Nat. Med.* **21**, 581–590 (2015). Medline doi:10.1038/nm.3838

32. D. A. Culton, S. K. McCray, M. Park, J. C. Roberts, N. Li, D. C. Zedek, G. J. Anhalt, D. O. Cowley, Z. Liu, L. A. Diaz, Mucosal pemphigus vulgaris anti-Dsg3 IgG is pathogenic to the oral mucosa of humanized Dsg3 mice. *J. Invest. Dermatol.* **135**, 1590–1597 (2015). Medline doi:10.1038/jid.2015.54

33. P. Katsamba, K. Carroll, G. Ahlsen, F. Bahna, J. Vendome, S. Posy, M. Rajebhosale, S. Price, T. M. Jessell, A. Ben-Shaul, L. Shapiro, B. H. Honig, Linking molecular affinity and cellular specificity in cadherin-mediated adhesion. *Proc. Natl. Acad. Sci. U.S.A.* **106**, 11594–11599 (2009). Medline doi:10.1073/pnas.0905349106

34. M. Hudecek, M. T. Lupo-Stanghellini, P. L. Kosasih, D. Sommermeyer, M. C. Jensen, C. Rader, S. R. Riddell, Receptor affinity and extracellular domain modifications affect tumor recognition by ROR1-specific chimeric antigen receptor T cells. *Clin. Cancer Res.* **19**, 3153–3164 (2013). Medline doi:10.1158/1078-0432.CCR-13-0330

35. K. Watanabe., S. Terakura, S. Uchiyama, A. C. Martens, T. van Meerten, H. Kiyoi, T. Nishida, T. Naoe, M. Murata, Excessively high-affinity single-chain fragment variable region in a chimeric antigen receptor can counteract T-cell proliferation. *Blood* **124**, 4799 (2014). http://www.bloodjournal.org/content/124/21/4799

36. S. Srivastava, S. R. Riddell, Engineering CAR-T cells: Design concepts. *Trends Immunol.* **36**, 494–502 (2015). Medline doi:10.1016/j.it.2015.06.004

37. H. Wardemann, S. Yurasov, A. Schaefer, J. W. Young, E. Meffre, M. C. Nussenzweig, Predominant autoantibody production by early human B cell precursors. *Science* **301**, 1374–1377 (2003). Medline doi:10.1126/science.1086907

38. L. S. Berberian, Y. Valles-Ayoub, L. K. Gordon, S. R. Targan, J. Braun, Expression of a novel autoantibody defined by the VH3-15 gene in inflammatory bowel disease and *Campylobacter jejuni* enterocolitis. *J. Immunol.* **153**, 3756–3763 (1994). Medline

39. A. S. Payne, K. Ishii, S. Kacir, C. Lin, H. Li, Y. Hanakawa, K. Tsunoda, M. Amagai, J. R. Stanley, D. L. Siegel, Genetic and functional characterization of human pemphigus vulgaris monoclonal autoantibodies isolated by phage display. *J. Clin. Invest.* **115**, 888–899 (2005). Medline doi:10.1172/JCI24185

40. M. J. Cho, A. S. Lo, X. Mao, A. R. Nagler, C. T. Ellebrecht, E. M. Mukherjee, C. M. Hammers, E. J. Choi, P. M. Sharma, M. Uduman, H. Li, A. H. Rux, S. A. Farber, C. B. Rubin, S. H. Kleinstein, B. S. Sachais, M. R. Posner, L. A. Cavacini, A. S. Payne, Shared VH1-46 gene usage by pemphigus vulgaris autoantibodies indicates common humoral immune responses among patients. *Nat. Commun.* **5**, 4167 (2014). Medline doi:10.1038/ncomms5167

41. G. Di Zenzo, G. Di Lullo, D. Corti, V. Calabresi, A. Sinistro, F. Vanzetta, B. Didona, G. Cianchini, M. Hertl, R. Eming, M. Amagai, B. Ohyama, T. Hashimoto, J. Sloostra, F. Sallusto, G. Zambruno, A. Lanzavecchia, Pemphigus autoantibodies generated through somatic mutations target the desmoglein-3 cis-interface. *J. Clin. Invest.* **122**, 3781–3790 (2012). Medline doi:10.1172/JCI64413

42. A. S. Payne, D. L. Siegel, J. R. Stanley, Targeting pemphigus autoantibodies through their heavy-chain variable region genes. *J. Invest. Dermatol.* **127**, 1681–1691 (2007). Medline doi:10.1038/sj.jid.5700790

43. X. Mao, H. Li, Y. Sano, M. Gaestel, J. Mo Park, A. S. Payne, MAPKAP kinase 2 (MK2)-dependent and -independent models of blister formation in pemphigus vulgaris. *J. Invest. Dermatol.* **134**, 68–76 (2014). Medline doi:10.1038/jid.2013.224

44. M. C. Milone, J. D. Fish, C. Carpenito, R. G. Carroll, G. K. Binder, D. Teachey, M. Samanta, M. Lakhal, B. Gloss, G. Danet-Desnoyers, D. Campana, J. L. Riley, S. A. Grupp, C. H. June, Chimeric receptors containing CD137 signal transduction domains mediate enhanced survival of T cells and increased antileukemic efficacy in vivo. *Mol. Ther.* **17**, 1453–1464 (2009). Medline doi:10.1038/mt.2009.83

45. X. Wu, Z. Y. Yang, Y. Li, C. M. Hogerkorp, W. R. Schief, M. S. Seaman, T. Zhou, S. D. Schmidt, L. Wu, L. Xu, N. S. Longo, K. McKee, S. O'Dell, M. K. Louder, D. L. Wycuff, Y. Feng, M. Nason, N. Doria-Rose, M. Connors, P. D. Kwong, M. Roederer, R. T. Wyatt, G. J. Nabel, J. R. Mascola, Rational design of envelope identifies broadly neutralizing human monoclonal antibodies to HIV-1. *Science* **329**, 856–861 (2010). Medline

46. R. Hassan, M. R. Lerner, D. Benbrook, S. A. Lightfoot, D. J. Brackett, Q. C. Wang, I. Pastan, Antitumor activity of SS(dsFv)PE38 and SS1(dsFv)PE38, recombinant antimesothelin immunotoxins against human gynecologic cancers grown in organotypic culture in vitro. *Clin. Cancer Res.* **8**, 3520–3526 (2002). Medline

47. E. Wang, L. C. Wang, C. Y. Tsai, V. Bhoj, Z. Gershenson, E. Moon, K. Newick, J. Sun, A. Lo, T. Baradet, M. D. Feldman, D. Barrett, E. Puré, S. Albelda, M. C. Milone, Generation of potent T-cell immunotherapy for cancer using DAP12-based, multichain, chimeric immunoreceptors. *Cancer Immunol. Res.* **3**, 815–826 (2015). Medline doi:10.1158/2326-6066.CIR-15-0054

48. E. Hooijberg, A. Q. Bakker, J. J. Ruizendaal, H. Spits, NFAT-controlled expression of GFP permits visualization and isolation of antigen-stimulated primary human T cells. *Blood* **96**, 459–466 (2000). Medline

49. S. Duffy, K. L. Tsao, D. S. Waugh, Site-specific, enzymatic biotinylation of recombinant proteins in *Spodoptera frugiperda* cells using biotin acceptor peptides. *Anal. Biochem.* **262**, 122–128 (1998). Medline doi:10.1006/abio.1998.2770

50. T. Funakoshi, L. Lunardon, C. T. Ellebrecht, A. R. Nagler, C. E. O'Leary, A. S. Payne, Enrichment of total serum IgG4 in patients with pemphigus. *Br. J. Dermatol.* **167**, 1245–1253 (2012). Medline doi:10.1111/j.1365-2133.2012.11144.x

51. T. E. Costa, R. R. Franke, M. Sanchez, Z. Misulovin, M. C. Nussenzweig, Functional reconstitution of an immunoglobulin antigen receptor in T cells. *J. Exp. Med.* **175**, 1669–1676 (1992). Medline doi:10.1084/jem.175.6.1669

52. M. Jonnalagadda, A. Mardiros, R. Urak, X. Wang, L. J. Hoffman, A. Bernanke, W. C. Chang, W. Bretzlaff, R. Starr, S. Priceman, J. R. Ostberg, S. J. Forman, C. E. Brown, Chimeric antigen receptors with mutated IgG4 Fc spacer avoid fc receptor binding and improve T cell persistence and antitumor efficacy. *Mol. Ther.* **23**, 757–768 (2015). Medline doi:10.1038/mt.2014.208

53. D. M. Barrett, A. E. Seif, C. Carpenito, D. T. Teachey, J. D. Fish, C. H. June, S. A. Grupp, G. S. Reid, Noninvasive bioluminescent imaging of primary patient acute lymphoblastic leukemia: A strategy for preclinical modeling. *Blood* **118**, e112–e117 (2011). Medline doi:10.1182/blood-2011-04-346528

54. L. A. Johnson, J. Scholler, T. Ohkuri, A. Kosaka, P. R. Patel, S. E. McGettigan, A. K. Nace, T. Dentchev, P. Thekkat, A. Loew, A. C. Boesteanu, A. P. Cogdill, T. Chen, J. A. Fraietta, C. C. Kloss, A. D. Posey Jr., B. Engels, R. Singh, T. Ezell, N. Idamakanti, M. H. Ramones, N. Li, L. Zhou, G. Plesa, J. T. Seykora, H. Okada, C. H. June, J. L. Brogdon, M. V. Maus, Rational development and characterization of humanized anti-EGFR variant III chimeric antigen receptor T cells for glioblastoma. *Sci. Transl. Med.* **7**, 275ra22 (2015). Medline doi:10.1126/scitranslmed.aaa4963

55. B. A. Schodin, T. J. Tsomides, D. M. Kranz, Correlation between the number of T cell receptors required for T cell activation and TCR-ligand affinity. *Immunity* **5**, 137–146 (1996). Medline doi:10.1016/S1074-7613(00)80490-2